Alpha-particle-induced reactions on natural silver in the 10-50 MeV energy range: production of ^{111}In, ^{110m}In and ^{109}Cd

Zolbadral Tsoodol [a,b], Masayuki Aikawa [c,d,e], Ichinkhorloo Dagvadorj [a], Damdinsuren Gantumur [d], He Huang [d], Hiromitsu Haba [f]

[a] *Nuclear Research Center, National University of Mongolia, Ulaanbaatar 13330, Mongolia*

[b] *New Mongolia College of Technology, Ulaanbaatar 13372, Mongolia*

[c] *Faculty of Science, Hokkaido University, Sapporo 060-0810, Japan*

[d] *Global Center for Biomedical Science and Engineering, Faculty of Medicine, Hokkaido University, Sapporo 060-8648, Japan*

[e] *Graduate School of Biomedical Science and Engineering, Hokkaido University, Sapporo 060-8638, Japan*

[f] *Nishina Center for Accelerator-Based Science, RIKEN, Wako 351-0198, Japan*

Abstract

Production cross sections of medical radionuclides ^{111}In, ^{110m}In and ^{109}Cd were investigated in the α-particle-induced reactions on natural silver up to 50 MeV. The stacked-foil activation technique and γ-ray spectrometry were used to determine the cross sections. The excitation functions of byproducts ^{104g,105,106m,110m}Ag, ^{107,111m}Cd and ^{107g,108g,108m,109,110g}In were also determined. Physical yields of ^{111}In, ^{110m}In and ^{109}Cd were deduced based on the measured cross sections.

Keywords

Indium-111; Indium-110m; Cadmium-109; Alpha-particle-induced reactions; Excitation function; Cross section; Physical yield

1 Introduction

Indium and cadmium radionuclides, such as ^{111}In, ^{110m}In and ^{109}Cd, can be used for nuclear medicine. Indium-111 ($T_{1/2}$ = 2.8047 d) decays via the electron capture process with emission of intense γ rays of 171.28 keV (I_γ = 90.7%) and 245.35 keV (I_γ = 94.1%). The radionuclide also emits 2.72-keV L-Auger line (100.4%) and 19.3-keV K-Auger line (15.5%). Due to its favorable half-life and decay properties, ^{111}In is used in diagnostic nuclear medicine and internal radiotherapy (Chow et al., 2008; Kassis, 2004). It is also employed in radiolabeled immunoglobulin treatment (Chow et al., 2008; Hu et al., 2007), labeling of monoclonal antibodies (Mitterhauser et al., 2003) and cellular blood components (Thakur, 1977), and cancer imaging (Misri et al., 2011). ^{111}In can be produced by bombarding enriched/natural cadmium and silver targets with protons, deuterons, and α-particles. The natural composition targets are economically desirable for production of medical isotopes. Using natural

cadmium targets, however, the production of the impurity ^{114m}In ($T_{1/2}$ = 49.51 d) could not be avoided at any projectile energy (Lahiri et al., 2013). Alternative production route for ^{111}In without the impurity ^{114m}In can be the (α,x) reaction on ^{nat}Ag (Tárkányi et al., 2015) .

The meta-stable state of indium-110 (^{110m}In) has a half-life of 69.1 min and emits a positron (E_{β^+} = 1011 keV, I_{β^+} = 61.3%). This radionuclide can be used to label proteins and peptides for positron emission tomography (PET) imaging (Lubberink et al., 2002; Tolmachev and Stone-Elander, 2010). ^{110m}In also emits the medium-energy and high-intensity γ line that is useful for β+γ coincidence PET (Sitarz et al., 2020). The ^{107}Ag(α,n)^{110m}In reaction is the promising candidate route for the ^{110m}In production (Tárkányi et al., 2015). The existing experimental data in our literature survey are inconsistent with each other and insufficient for investigating this production route above 30 MeV.

Cadmium-109 ($T_{1/2}$ = 461.9 d) decays to ^{109m}Ag ($T_{1/2}$ = 39.79 s, IT = 100%) via only the electron capture process. ^{109}Cd is commonly used as a calibration source for X-ray and γ-ray detectors, and a radioactive tracer for environmental study of Cd pollutant (Aardaneh et al., 2008; Landini and Osso, 2001). Morewover, this radionuclide can be considered as a generator of ^{109m}Ag, which emits 88.03-keV γ rays suitable for single photon emission computed tomography (SPECT) (Faßbender et al., 2004; Mansur et al., 1995; Mirzaii et al., 2009). Possible production routes of ^{109}Cd are charged-particle-induced reactions on silver, cadmium, indium and palladium targets (Tárkányi et al., 2018). Among these production routes, the ^{nat}Ag(α,x)^{109}Cd reaction is considered as a promising one. However, the experimental results of the ^{nat}Ag(α,x)^{109}Cd reaction are largely scattered.

The cross sections of the α-particle-induced reactions on a natural silver target are thus related to medical radioisotope production. The availability of the reactions in practical use can be discussed based on the experimental cross sections. Accurate experimental cross sections are indispensable for the discussion to obtain enough amount of the radioisotope of interest and to suppress production of unnecessary co-products. However, the experimental cross sections published earlier are scattered and less consistent. Therefore, this work aims to measure reliable energy-dependent cross sections of the α-particle-induced reaction on natural silver. The production cross sections of ^{104g,105,106m,110m}Ag, ^{107,109,111m}Cd and ^{107g,108g,108m,109,110g,110m,111}In were determined. The results are expected to contribute to the selection of the production route of the medical radioisotopes.

2 Experimental methods

The experiment was performed at the AVF cyclotron of RIKEN RI Beam Factory. The stacked-foil activation technique and γ-ray spectrometry were used to measure the cross sections.

The stacked target consisted of thin and pure metallic foils of ^{nat}Ag (99.9% purity, Nilaco Corp., Japan) and ^{nat}Ti (99.6% purity, Nilaco Corp., Japan). The average thicknesses of the foils were derived by measuring the weight and size of the original foils. The derived thicknesses of the ^{nat}Ag and ^{nat}Ti foils were 10.1 mg/cm^2 and 2.23 mg/cm^2, respectively. The targets of 10×10 mm dimensions were cut and arranged into the target holder,

which served as a Faraday cup. The stacked target consisted of 13 sets of the Ti-Ag-Ag-Ag foil. The second and third Ag foils in each set were used as main targets taking into account compensation of recoiled reaction products from the Ag foils at the beam upstream. The Ti foils served for monitoring the beam parameters via the $^{nat}Ti(\alpha,x)^{51}Cr$ reaction.

The stacked target was irradiated for 30 min with an α-particle beam with incident energy of 50.3 ± 0.2 MeV, determined by the time-of-flight method (Watanabe et al., 2014). The average beam current determined by irradiation time and the collected charge with the Faraday cup was 212 nA. The beam energy loss in the stacked target was calculated using stopping power derived from the SRIM code (Ziegler et al., 2010).

The γ-ray spectra of each irradiated foil were measured by a high-resolution HPGe detector (ORTEC GMX30P4-70) without chemical separation and analyzed by the Gamma Studio software (SEIKO EG&G). The detector was calibrated by a mixed γ-ray point source containing $^{57,60}Co$, ^{85}Sr, ^{88}Y, ^{109}Cd, ^{113}Sn, ^{137}Cs, ^{139}Ce, ^{203}Hg, and ^{241}Am. Several series of γ-ray measurements were performed to follow the decay of the produced isotopes. Each foil was measured more than three times in 3 months. The distance between the detector and the foils was arranged to keep the dead time less than 5%. The nuclear reaction and decay data for the γ-ray spectrometry were taken from NuDat 3.0 (National Nuclear Data Center, 2019), LiveChart (International Atomic Energy Agency, 2009; Verpelli and Abriola, 2011) and QCalc (Pritychenko and Sonzogni, 2003). The data for all possible contributing reaction channels for the formation of radionuclides of interest are listed in Table 1.

The primary beam parameters and target thicknesses were cross-checked using the $^{nat}Ti(\alpha,x)^{51}Cr$ monitor reaction. The cross sections of the $^{nat}Ti(\alpha,x)^{51}Cr$ monitor reaction were derived from the measurements of the 320.08-keV γ rays (I_γ = 9.91%) emitted in the ^{51}Cr decay ($T_{1/2}$ = 27.704 d). Each Ti foil was measured with the next Ag catcher foil. There was an overlapping contribution from the decay of ^{105}Ag ($T_{1/2}$ = 41.3 d), which emits the γ line at 319 keV (I_γ = 4.35%) above the threshold energy of 18 MeV. The contribution of ^{105}Ag could be found in the spectra above 25 MeV. Therefore, the cross sections below 25 MeV were compared with the IAEA recommended values (Hermanne et al., 2018; Takács et al., 2007). To obtain a better agreement between the measured excitation function and the IAEA recommended values, the measured initial beam energy was corrected by +0.2 MeV within the uncertainty. The measured thicknesses of the Ti and Ag foils were corrected by -1% within the uncertainty. The cross sections using the corrected parameters are in good agreement with the recommended values as presented in Fig. 1. The corrected projectile energy (50.5 ± 0.2 MeV) and thicknesses (10.0 and 2.21 mg/cm^2 for Ag and Ti foils, respectively) were adopted for the following analysis.

The uncertainty of the projectile energy is propagated to ± 1.1 MeV in the last foil of the stack, which was estimated from uncertainties of the incident energy (± 0.2 MeV) and target thicknesses (1%). The energy loss of 0.4-1.3 MeV in the foils was obtained using stopping power of the SRIM code. The midpoint projectile energy, total uncertainty and energy loss at each foil are listed in Table 2.

The total uncertainty of the cross sections was 7.1-41.1%. It was calculated as the square root of the quadratic summation of the components: beam intensity (5%), target thickness (1%), target purity (1%), detector efficiency (5%), γ-ray intensity (<3%), and γ-ray counting (0.4-40%).

3 Results and discussion

The activation cross sections of ^{104g,105,106m,110m}Ag, ^{107,109,111m}Cd and ^{107g,108g,108m,109,110g,110m,111}In were measured for the α-particle-induced reactions on ^{nat}Ag. The results with total uncertainties are summarized in Table 2 and displayed in Figs. 2-15, in comparison with the previous experimental values using ^{nat}Ag (Chaubey et al., 1990; Ditrói et al., 2018; Fukushima et al., 1965; Fuqing et al., 1994; Guin et al., 1992; Ismail and Divatia, 1988; Mukhrjee et al., 1991; Peng et al., 1996; Porges, 1956; Shahid et al., 2017; Singh et al., 1987; Takács et al., 2010; Tárkányi et al., 2015; Wasilevsky et al., 1988, 1985a, 1985b), and the theoretical prediction of TENDL-2021 (Koning et al., 2019). The literature data normalized to enriched isotope targets were renormalized appropriately to those on natural targets for comparison in the figures.

3.1 Cumulative cross sections of the ^{nat}Ag(α,x)^{111g}In reaction

The short-lived meta-stable state ($T_{1/2}$ = 7.7 min) and the long-lived ground state ($T_{1/2}$ = 2.8047 d) of ^{111}In are simultaneously formed through the (α,γ) reaction on ^{107}Ag and the (α,2n) reaction on ^{109}Ag in natural silver. The meta-stable state decayed by the internal transition (IT) (100%) into the ground state during a cooling time of about 1 day. The cumulative cross sections of the ^{nat}Ag(α,x)^{111g}In reaction were derived from the measurements of the intense 171.28-keV γ rays (I_γ = 90.7 %) emitted from the decay of the ground state. An overlapping contribution of the 171.34-keV γ rays (I_γ = 0.056%) emitted from ^{105}Cd ($T_{1/2}$ = 55.5 min) into the photo peak at 171.28 keV was negligible due to its short half-life and weak intensity. Based on measurements of another γ line at 245.35 keV (I_γ= 94.1%), the internal consistency was confirmed.

The excitation function is shown in Fig. 2 in comparison with the theoretical prediction of TENDL-2021 (Koning et al., 2019) and the previous experimental data on natural silver targets (Chaubey et al., 1990; Ditrói et al., 2018; Fukushima et al., 1965; Fuqing et al., 1994; Guin et al., 1992; Ismail and Divatia, 1988; Mukhrjee et al., 1991; Peng et al., 1996; Porges, 1956; Shahid et al., 2017; Singh et al., 1987; Takács et al., 2010; Tárkányi et al., 2015; Wasilevsky et al., 1985a). The present results show overall agreement with the measured values except for the data reported by Wasilevsky et al. (1985a). The TENDL-2021 prediction underestimates the experimental values at the peak of the excitation function.

3.2 Independent cross sections of the ^{nat}Ag(α,x)^{110m}In reaction

The meta-stable state of ^{110}In ($T_{1/2}$ = 69.1 min) can directly be formed by the (α,n) reaction with E_{thr} = 7.81 MeV on ^{107}Ag and the (α,3n) reaction with E_{thr} = 24.74 MeV on ^{109}Ag in the natural silver targets. Hence, two peaks below 50 MeV were observed. With no indirect way to produce ^{110m}In, the independent cross sections of the ^{nat}Ag(α,x)^{110m}In reaction could be determined. The intense 657.75-keV γ rays (I_γ = 97.4 %) emitted from the decay of ^{110m}In were used for the data assessment. After cooling times of 1-3 hours, the γ-rays from the irradiated foils were measured. The γ line was possibly interfered with γ rays of 657.8 keV (I_γ = 95.61%) in the decay of

^{110m}Ag ($T_{1/2}$ = 249.83 d) and of 657.53 (I_γ = 0.070%) and 658.27 keV (I_γ = 0.03%) in the decay of ^{105}Cd ($T_{1/2}$ = 55.5 min). The interferences were neglected due to the long half-life of ^{110m}Ag and weak intensities of ^{105}Cd, respectively. The contribution to the same γ line (I_γ = 98%) from the decay of ^{110g}In ($T_{1/2}$ = 4.9 h) was subtracted taking into account the detector efficiencies, the γ-ray intensities, and the measured net counts of another γ line at 884.667 keV (I_γ = 93.0 %). The internal consistency among the series of the activity measurements was confirmed.

The obtained excitation function of the ^{nat}Ag(α,x)^{110m}In reaction is shown in Fig. 3 in comparison with previously measured cross sections on natural silver targets (Chaubey et al., 1990; Ditrói et al., 2018; Fukushima et al., 1965; Peng et al., 1996; Shahid et al., 2017; Takács et al., 2010; Tárkányi et al., 2015; Wasilevsky et al., 1985b), and the theoretical prediction of TENDL-2021 (Koning et al., 2019). The most data are consistent with our results. At the first peak below 25 MeV, the position of data reported by Takács et al. (2010) is slightly higher than our results. The data reported by Ditrói et al. (2018) at the second peak are much higher than other measured values. The excitation function extracted from the TENDL-2021 library is higher than our results above 25 MeV.

3.3 Independent cross sections of the ^{nat}Ag(α,x)^{110g}In reaction

Independent cross sections of the ^{nat}Ag(α,x)^{110g}In reaction were derived from the measurements of the intense 884.667-keV γ rays (I_γ = 93.0 %) emitted from the decay of ^{110g}In ($T_{1/2}$ = 4.9 h). The γ-ray measurements were performed after a cooling time of 3-5 hours. The contribution of the same γ line (I_γ = 75.0 %) emitted from ^{110m}Ag ($T_{1/2}$ = 249.83 d) was negligibly small due to its longer half-life. In addition, contributions from γ-rays of 884.7 keV (I_γ = 0.16 %) emitted from ^{110m}In ($T_{1/2}$ = 69.1 min), 884.1 keV (I_γ = 0.28%) from ^{108m}In ($T_{1/2}$ = 39.6 min), and 884.57 keV (I_γ = 0.59%) from ^{105}Cd ($T_{1/2}$ = 55.5 min) were neglected due to their weaker intensities. The internal consistency was confirmed using the 937.478-keV γ line (I_γ= 68.4 %).

The obtained excitation function of the ^{nat}Ag(α,x)^{110g}In reaction is compared with previously measured cross sections on natural silver targets (Chaubey et al., 1990; Ditrói et al., 2018; Fukushima et al., 1965; Fuqing et al., 1994; Guin et al., 1992; Porges, 1956; Shahid et al., 2017; Singh et al., 1987; Takács et al., 2010; Tárkányi et al., 2015; Wasilevsky et al., 1985b), and the theoretical prediction of TENDL-2021 (Koning et al., 2019) in Fig. 4. Our results are consistent with all the previous data within the uncertainty except for the data of Wasilevsky et al. (1985b), and Singh et al. (1987) above 30 MeV. The TENDL-2021 prediction underestimates the experimental data, and its peak position is slightly shifted to the lower energy side.

3.4 Cumulative cross sections of the ^{nat}Ag(α,x)^{109g}In reaction

^{109g}In ($T_{1/2}$ = 4.167 h) can be formed directly in the (α,2n) reaction on ^{107}Ag and the (α,4n) reaction on ^{109}Ag and indirectly from the decays of the short-lived excited states of ^{109}In at 0.650 MeV ($T_{1/2}$ = 1.34 min, IT: 100%) and 2.101 MeV ($T_{1/2}$ = 0.209 s, IT: 100%). The cumulative cross sections of the ^{nat}Ag(α,x)^{109g}In reaction were

derived from the measurements of 203.3-keV γ rays (I_γ = 74.2 %) after a cooling time of 3-5 hours. An overlapping peak at 204.95 keV (I_γ = 47.2%) emitted from ^{107g}In ($T_{1/2}$ = 32.4 min) in the spectra was properly separated. The contribution of 202.21-keV γ rays (I_γ = 0.029%) from ^{105}Ag ($T_{1/2}$ = 41.29 d) was negligibly small due to its long half-life and weak intensity. The internal consistency was checked using the γ line at 1148.5 keV (I_γ = 4.67 %) emitted from the ^{109g}In.

Figure 5 shows the obtained excitation function of the ^{nat}Ag(α,x)^{109g}In reaction in comparison with previously measured cross sections on natural silver (Chaubey et al., 1990; Ditrói et al., 2018; Guin et al., 1992; Mukhrjee et al., 1991; Peng et al., 1996; Porges, 1956; Shahid et al., 2017; Singh et al., 1987; Takács et al., 2010; Wasilevsky et al., 1985a), and the theoretical prediction of TENDL-2021 (Koning et al., 2019). The data reported by Chaubey et al. (1990) are lower than our data at the first peak. The peak position of the data of Wasilevsky et al. (1985a) is shifted to the higher energy. The shape of the excitation function extracted from the TENDL-2021 library is in partial agreement with all the experimental datasets.

3.5 Independent cross sections of the ^{nat}Ag(α,x)^{108m}In reaction

The meta-stable state of ^{108m}In ($T_{1/2}$ = 39.6 min) can directly be formed through the (α,3n) reaction on ^{107}Ag and the (α,5n) reaction on ^{109}Ag in natural silver targets. ^{108m}In decays through the electron capture and β decay modes (100%) into ^{108}Cd and no internal transition mode into ^{108g}In. The measurements of 632.9-keV γ line (I_γ = 76.4 %) after a short cooling time of 1-3 hours were used to deduce the independent cross sections of the ^{nat}Ag(α,x)^{108m}In reaction. The intense γ line was interfered with the same γ line (I_γ = 100%) emitted from ^{108g}In ($T_{1/2}$ = 58.0 min). The contribution of ^{108g}In was properly subtracted using the net counts of another γ line of 875.4 keV (I_γ = 100%) from ^{108g}In.

The obtained excitation function of the ^{nat}Ag(α,x)^{108m}In reaction is shown in Fig. 6 in comparison with previous experimental data on natural silver targets (Ditrói et al., 2018; Shahid et al., 2017; Takács et al., 2010; Wasilevsky et al., 1985b), and the theoretical prediction of TENDL-2021 (Koning et al., 2019). Above 35 MeV, our results are lower than previously measured values. The peak position of the data of Wasilevsky et al. (1985b) is shifted to the higher energy. The shape of the excitation function of the TENDL-2021 prediction is similar to that of our results.

3.6 Independent cross sections of the ^{nat}Ag(α,x)^{108g}In reaction

Several γ rays emitted from ^{108g}In ($T_{1/2}$ = 58.0 min) are listed in Table 1. Among them, the stronger and interference-free γ line at 1032.8 keV (I_γ = 35 %) was adopted. The independent cross sections of the ^{nat}Ag(α,x)^{108g}In reaction were derived. The internal consistency could not be confirmed among different γ rays emitted from the ^{108g}In decay. The cross sections using the 1032.8-keV γ line are smaller than those using others, which may indicate less interference from the ^{108m}In decay. The inconsistency may be caused by a large

uncertainty of the γ-ray intensity (~10 %).

The obtained excitation function of the $^{nat}Ag(\alpha,x)^{108g}In$ reaction is compared with the previous experimental data on natural silver targets (Ditrói et al., 2018; Shahid et al., 2017; Takács et al., 2010; Wasilevsky et al., 1985b), and the theoretical prediction of TENDL-2021 (Koning et al., 2019) in Fig. 7. Present results are in good agreement with data reported by Shahid et al. (2017) and are consistent with data reported by Ditrói et al. (2018) and Takács et al. (2010) within the uncertainty. The data reported by Wasilevsky et al. (1985b) shift to the higher energy. The TENDL-2021 prediction shows partial agreement with our data and its peak position shifts to the lower energy side.

3.7 Cumulative cross sections of the $^{nat}Ag(\alpha,x)^{107g}In$ reaction

^{107g}In ($T_{1/2}$ = 32.4 min) could be directly produced through the (α,4n) reaction on ^{107}Ag with E_{thr} = 35.74 MeV in natural silver targets. The cross sections are cumulative regarding indirect contribution from an excited state at 0.679 MeV of ^{107}In ($T_{1/2}$ = 50.4 s, IT: 100%). The measurements of the 204.45-keV γ line (I_γ = 47.2 %), which overlapped with the peak at 203.3 keV (I_γ = 74.2%) from ^{109g}In ($T_{1/2}$ = 4.2 h), were used in data assessments. The interfered peak was properly separated. The internal consistency was checked with the γ rays of 320.94 keV (I_γ= 10.2 %) emitted from ^{107g}In. The consistency with the results using the other γ lines and measurement series was confirmed.

The obtained excitation function is compared with previous experimental data on natural silver targets (Wasilevsky et al., 1985a), and theoretical prediction of TENDL-2021 (Koning et al., 2019) in Fig. 8. Our results are inconsistent with the data of Wasilevsky et al. (1985a). The TENDL-2021 prediction underestimates our experimental data.

3.8 Independent cross sections of the $^{nat}Ag(\alpha,x)^{111m}Cd$ reaction

The meta-stable state of ^{111}Cd ($T_{1/2}$ = 48.5 min) can be formed directly in the (α,d) and (α,np) reactions on ^{109}Ag in natural silver targets. Most of the co-produced ^{111g}In ($T_{1/2}$ = 2.8047 d, EC: 100 %), ^{111m}Ag ($T_{1/2}$ = 64.8 s, β^-: 0.7 %) and ^{111g}Ag ($T_{1/2}$ = 7.45 d, β^-: 100 %) decay only to the ground state of ^{111}Cd. The branching ratio of the co-products decay to ^{111m}Cd is negligible. The independent cross sections of $^{nat}Ag(\alpha,x)^{111m}Cd$ reaction were derived based on the measurements of 150.825-keV γ rays (I_γ = 29.1 %) after a short cooling time of 1-3 hours. The interference from the ^{111g}In ($T_{1/2}$ = 2.8047 d) decay can be neglected due to its long half-life and tiny branching ratio (0.003%).

The obtained excitation function of the $^{nat}Ag(\alpha,x)^{111m}Cd$ reaction is presented in Fig. 9 in comparison with previously measured cross sections on natural silver targets (Shahid et al., 2017; Takács et al., 2010) and the theoretical prediction of TENDL-2021 (Koning et al., 2019). Our results are in good agreement with data reported by Takács et al. (2010) and slightly larger than the data reported by Shahid et al. (2017). The excitation

function in the TENDL-2021 prediction agrees with the data of Shahid et al. (2017) but disagree with the other experimental datasets.

3.9 Cumulative cross sections of the ^{nat}Ag(α,x)^{109}Cd reaction

The long-lived radionuclide ^{109}Cd ($T_{1/2}$ = 461.4 d) can be formed directly by several channels listed in Table 1 and indirectly through decay of the simultaneously produced ^{109g}In ($T_{1/2}$ = 4.167 h, EC: 100 %). The cumulative cross sections of the ^{nat}Ag(α,x)^{109}Cd reaction were derived from the measurements of only one detectable γ ray of 88.0336 keV (I_γ = 3.644 %) emitted in decay of ^{109}Cd. The γ-spectra measurements were performed after a longer cooling time of around 50 days. There are possible interferences of X rays at 87.300 keV (I_γ = 3.90%) and 87.580 keV (I_γ = 0.88%) of the Pb shielding. The X-ray interferences could be ignored because no peak of the more intense X ray at 74.969 keV (I_γ = 46.8%) was observed in the spectra. The self-absorption correction (Alfassi et al., 2009) for this low energy γ rays was taken into account using the mass attenuation coefficient of 2.18 cm^2/g for the γ line at 88.0336 keV (Hubbel and Seltzer, 2004). The self-absorption was estimated to be 1.1%.

The obtained excitation function is shown in Fig. 10 in comparison with the previously measured cross sections on natural silver targets (Ditrói et al., 2018; Peng et al., 1996; Porges, 1956; Tárkányi et al., 2018), and the theoretical prediction of TENDL-2021 (Koning et al., 2019). presentresults agree with data reported by Ditrói et al. (2018), Tárkányi et al. (2018), and Porges (1956) within the uncertainty. The data reported by Peng et al. (1996) are much lower than other experimental datasets. The data in TENDL-2021 underestimate the amplitude at the first peak.

3.10 Cumulative cross sections of the ^{nat}Ag(α,x)^{107}Cd reaction

In addition to direct reactions listed in Table 1, ^{107}Cd ($T_{1/2}$ = 6.5 h) could be indirectly formed from the decay of co-produced ^{107}In ($T_{1/2}$ = 32.4 min, EC: 100 %). After the cooling time of 5-20 hours, the cumulative cross sections were derived from the measurements of an interference-free γ ray of 93.124 keV (I_γ = 4.7 %) emitted from ^{107}Cd. Based on the mass attenuation coefficient of 1.88 cm^2/g for the γ line at 93.124 keV (Hubbel and Seltzer, 2004), the self-absorption was estimated to be 1.1%. The internal consistency among the series of the activity measurements was confirmed.

The obtained excitation function is shown in Fig. 11 in comparison with the theoretical prediction of TENDL-2021 (Koning et al., 2019). The previous experimental data for the ^{nat}Ag(α,x)^{107}Cd reaction are not available in the investigated energy range. The TENDL-2021 prediction shows partial agreement with our experimental results.

3.11 Independent cross sections of the ^{nat}Ag(α,x)^{110m}Ag reaction

The long-lived meta-stable state of ^{110}Ag ($T_{1/2}$ = 249.83 d) can be formed directly in the (α,x) reactions on

^{nat}Ag as listed in Table 1. The measurements of the intense γ line of 657.76 keV (I_γ = 95.61%) after a long cooling time of around 50 days were used in data assessments. The contributions to the same γ line from ^{110g}In ($T_{1/2}$ = 4.9 h) and ^{110m}In ($T_{1/2}$ = 69.1 min) were negligible because they completely decayed during the long cooling time. The consistency of the result was confirmed using another γ line at 884.78 keV (I_γ= 75 %) emitted from ^{110m}Ag.

The obtained excitation function of the ^{nat}Ag(α,x)^{110m}Ag reaction is shown in Fig. 12. The results are compared with the previously measured cross sections on natural silver targets (Ditrói et al., 2018; Shahid et al., 2017; Takács et al., 2010; Wasilevsky et al., 1988), and the theoretical prediction of TENDL-2021 (Koning et al., 2019). Our results are comparable with all the measured values. The excitation function extracted from the TENDL-2021 library is in partial agreement with our results.

3.12 Independent cross sections of the ^{nat}Ag(α,x)^{106m}Ag reaction

In our investigated energy range, ^{106m}Ag ($T_{1/2}$ = 8.28 d) can be formed directly by several nuclear reactions in natural silver targets listed in the Table 1. The measurements of the interference-free γ rays at 450.976 keV (I_γ = 95.61%) after a cooling time of 1.9-2.5 days were used in data assessments. The internal consistency was confirmed with the 1045.83-keV γ line (I_γ= 29.6 %) emitted from ^{106m}Ag.

The obtained excitation function of the ^{nat}Ag(α,x)^{106m}Ag reaction is shown in Fig. 13 and compared with the previous experimental data on natural silver targets (Ditrói et al., 2018; Shahid et al., 2017; Singh et al., 1987; Takács et al., 2010; Wasilevsky et al., 1988), and the theoretical prediction of TENDL-2021 (Koning et al., 2019). The peak position of the data reported by Wasilevsky et al. (1988) shifts to the higher energy. Our results agree with the other experimental values within the uncertainty and the TENDL-2021 prediction.

3.13 Cumulative cross sections of the ^{nat}Ag(α,x)^{105g}Ag reaction

^{105g}Ag ($T_{1/2}$ = 8.28 d) can be formed directly through several nuclear reactions listed in Table 1. It can also be formed indirectly by the decays of ^{105}Cd ($T_{1/2}$ = 55.5 min, ε+β$^+$: 100%) and ^{105m}Ag ($T_{1/2}$ = 7.23 min, ε+β$^+$: 0.34% and IT: 99.66%). The cumulative cross sections of the ^{nat}Ag(α,x)^{105g}Ag reaction were derived from the measurements of the interference free γ rays of 280.54 keV (I_γ = 31 %) and 344.61 keV (I_γ= 42 %) emitted from ^{105g}Ag. The cross sections deduced from several series of the activity measurements and different γ lines were consistent.

The obtained excitation function of the ^{nat}Ag(α,x)^{105g}Ag reaction is shown in Fig. 14 in comparison with the previous experimental data on natural silver targets (Ditrói et al., 2018; Guin et al., 1992; Ismail and Divatia, 1988; Shahid et al., 2017; Singh et al., 1987; Takács et al., 2010; Wasilevsky et al., 1988), and the theoretical prediction of TENDL-2021 (Koning et al., 2019). Present results agree with the experimental data other than those reported by Singh et al. (1987) and Wasilevsky et al. (1988). The TENDL-2021 prediction underestimates

all the measured cross sections.

3.14 Independent cross sections of the $^{nat}Ag(\alpha,x)^{104g}Ag$ reaction

^{104g}Ag ($T_{1/2}$ = 69.2 min) can be formed directly through several nuclear reactions listed in the Table 1. The production cross sections of ^{104g}Ag can be regarded as independent ones because of only negligible contribution from ^{104m}Ag ($T_{1/2}$ = 33.5 min, $\varepsilon+\beta^+$: 99.93% and IT: <0.07%). The measurements of γ rays of 767.6 keV (I_γ = 65.7%) emitted from ^{104g}Ag were used in the data assessment.

The obtained excitation function of the $^{nat}Ag(\alpha,x)^{104g}Ag$ reaction is compared with the data normalized from the previously measured cross sections (Guin et al., 1992; Wasilevsky et al., 1988) and the theoretical prediction of TENDL-2021 (Koning et al., 2019) in Fig. 15. One data point reported by Guin et al. (1992) at 48.3 MeV is in good agreement with our data. Our measured cross sections agree with the data reported by Wasilevsky et al. (1988) within the uncertainty. The TENDL-2021 prediction shows partial agreement with our results.

3.15 Integral Yield

The physical yields of ^{111}In, $^{110m,110g}In$, and ^{109}Cd were deduced based on the measured excitation functions and the stopping powers calculated using the SRIM code (Ziegler et al., 2010) according to the definition (Otuka and Takács, 2015). The results are shown in Figs. 16-18 with the previous experimental data (Dmitriev, 1986) up to 50 MeV.

The deduced physical yield of ^{111}In is shown in Fig. 16 and compared with the experimental data (Dmitriev, 1986). Our deduced physical yield is in partial agreement with data reported by Dmitriev (1986). The (α,2n) reaction on ^{109}Ag dominantly contributes to ^{111}In formation. To reduce co-produced indium isotopes, enriched ^{109}Ag targets and the beam energy window between the threshold energies of the $^{109}Ag(\alpha,2n)^{111}In$ (E_{thr} = 14.45 MeV) and $^{109}Ag(\alpha,3n)^{110}In$ (E_{thr} = 24.74 MeV) reactions can be considered. The physical yield of ^{111}In reaches at 9 MBq/μAh in this condition.

Figure 17 shows the deduced physical yields of $^{110m,110g}In$ in comparison with the previous experimental data of $^{110m,110g}In$ (Dmitriev, 1986). Our deduced physical yield of ^{110g}In is close to the experimental data reported by Dmitriev (1986). For ^{110m}In, data reported by Dmitriev (1986) are much lower than our deduced physical yield. The physical yield of ^{110m}In is greater than that of ^{110g}In below 45 MeV. Thus, a higher isomeric ratio can be achieved with lower projectile energy. In this production route, isotopic impurities ^{111}In and ^{109}In can be formed by the (α,2n) reaction on ^{109}Ag (E_{thr} = 14.45 MeV) and the (α,2n) reaction on ^{107}Ag (E_{thr} = 16.10 MeV), respectively. Therefore, ^{110m}In without contaminations from co-formed ^{111}In and ^{109}In can be produced by the (α,n) reaction on enriched ^{107}Ag in the energy range of 7.8-16.1 MeV.

The deduced physical yield of ^{109}Cd is shown in Fig. 18 in comparison with the previous experimental data (Dmitriev, 1986). Our deduced data are in agreement with the measured values reported by Dmitriev (1986). The deduced physical yield is 0.05 MBq/μAh in the 16-30 MeV energy range. This value is comparable with

that of the $^{nat}Ag(p,x)^{109}Cd$ reaction (0.07 MBq/μAh at 24 MeV) (Landini and Osso, 2001; Mirzaii et al., 2009). The co-produced ^{111m}Cd ($T_{1/2}$ = 48.5 min) and ^{107}Cd ($T_{1/2}$ = 5.6 h) can be easily eliminated thanks to their short half-lives. Production of ^{109}Cd with high radionuclidic purity is thus feasible.

4 Conclusion

The excitation functions of the α-particle-induced reactions on ^{nat}Ag were measured up to 50 MeV with the special focus on the ^{111}In, ^{110m}In and ^{109}Cd production. The stacked-foil activation technique and the high-resolution γ-ray spectrometry were used for the cross-section measurements. The obtained results were compared with the previous experimental data and the theoretical predictions in the TENDL-2021 library. The measured excitation functions of the $^{nat}Ag(\alpha,x)^{111}In$, $^{nat}Ag(\alpha,x)^{110m}In$, and $^{nat}Ag(\alpha,x)^{109}Cd$ reactions are consistent with most of the previously published values. The physical yields are deduced from the measured cross sections. The radionuclidically pure ^{109}Cd can be produced by the α-particle-induced reaction on natural silver by applying proper cooling time and chemical separation.

Acknowledgements

The experiment was carried out at RI Beam Factory operated by RIKEN Nishina Center and CNS, University of Tokyo, Japan. This work was supported by Mongolian Foundation for Science and Technology under grant number 2022/159.

Declarations of interest

None.

References

Aardaneh, K., Naidoo, C., Steyn, G.F., 2008. Radiochemical separation of ^{109}Cd from a silver target. J Radioanal Nucl Chem 276, 831–834. https://doi.org/10.1007/s10967-008-0640-8

Alfassi, Z.B., Persico, E., Groppi, F., Bonardi, M.L., 2009. On the photon self-absorption correction for thin-target-yields vs. thick-target-yields in radionuclide production. Applied Radiation and Isotopes 67, 240–242. https://doi.org/10.1016/j.apradiso.2008.10.004

Chaubey, A.K., Bhardwaj, M.K., Gautam, R.P., Singh, R.K.Y., Ansari, M.A., Rizvi, I.A., Singh, H., 1990. Pre-equilibrium decay process in the alpha induced reactions of silver isotopes. Int J Rad Appl Instrum A 41, 401–405. https://doi.org/https://doi.org/10.1016/0883-2889(90)90150-F

Chow, T.H., Lin, Y.Y., Hwang, J.J., Wang, H.E., Tseng, Y.L., Pang, V.F., Wang, S.J., Whang-Peng, J., Ting, G., 2008. Diagnostic and therapeutic evaluation of ^{111}In-vinorelbine-liposomes in a human colorectal carcinoma HT-29/luc-bearing animal model. Nucl Med Biol 35, 623–634. https://doi.org/10.1016/J.NUCMEDBIO.2008.04.001

Ditrói, F., Takács, S., Haba, H., Komori, Y., Aikawa, M., Saito, M., Murata, T., 2018. Investigation of alpha particle induced reactions on natural silver in the 40–50 MeV energy range. Nucl Instrum Methods Phys Res B 436, 119–129. https://doi.org/10.1016/j.nimb.2018.09.018

Dmitriev, P.P., 1986. Radionuclide yield in reactions with protons, deuterons, alpha particles and helium 3. Report INDC(CCP) - 263. International Atomic Energy Agency.

Faßbender, M., Nortier, F.M., Phillips, D.R., Hamilton, V.T., Heaton, R.C., Jamriska, D.J., Kitten, J.J., Pitt, L.R., Salazar, L.L., Valdez, F.O., Peterson, E.J., 2004. Some nuclear chemical aspects of medical generator nuclide production at the Los Alamos hot cell facility. Radiochim Acta 92, 237–243. https://doi.org/10.1524/ract.92.4.237.35596

Fukushima, S., Kume, S., Okamura, H., Otozai, K., Sakamoto, K., Yoshizawa, Y., Hayashi, S., 1965. Excitation functions for the reactions induced by alpha particles on Ag109. Nuclear Physics 69, 273–290. https://doi.org/10.1016/0029-5582(65)90051-9

Fuqing, H., Xianguan, L., Mantian, L., Peng, X., 1994. Excitation functions for ^{107}Ag(α,n)^{110m}In, ^{107}Ag(α,2n)^{109}In, ^{107}Ag(α,pn)^{109}Cd and ^{109}Ag(α,2n)^{111}In reactions. Atomic Energy Science and Technology 28, 513–518.

Guin, R., Saha, S.K., Prakash, S., Uhl, M., 1992. Isomeric yield ratios and excitation functions in α-induced reactions on ^{107,109}Ag. Phys Rev C 46, 250–257. https://doi.org/10.1103/PhysRevC.46.250

Hermanne, A., Ignatyuk, A. V., Capote, R., Carlson, B. V., Engle, J.W., Kellett, M.A., Kibédi, T., Kim, G., Kondev, F.G., Hussain, M., Lebeda, O., Luca, A., Nagai, Y., Naik, H., Nichols, A.L., Nortier, F.M., Suryanarayana, S. V., Takács, S., Tárkányi, F.T., Verpelli, M., 2018. Reference Cross Sections for Charged-particle Monitor Reactions. Nuclear Data Sheets 148, 338–382. https://doi.org/10.1016/j.nds.2018.02.009

Hu, M., Scollard, D., Chan, C., Chen, P., Vallis, K., Reilly, R.M., 2007. Effect of the EGFR density of breast

cancer cells on nuclear importation, in vitro cytotoxicity, and tumor and normal-tissue uptake of [111In] DTPA-hEGF. Nucl Med Biol 34, 887–896. https://doi.org/10.1016/J.NUCMEDBIO.2007.06.010

Hubbel, J.H., Seltzer, S.M., 2004. X-Ray Mass Attenuation Coefficients: NIST Standard Reference Database 126 [WWW Document]. https://doi.org/10.18434/T4D01F

International Atomic Energy Agency, 2009. LiveChart of Nuclides. [WWW Document]. URL https://www-nds.iaea.org/livechart/.

Ismail, M., Divatia, A.S., 1988. Measurement and analysis of alpha-induced reactions on Ta, Ag and Co. Pramana 30, 193–210. https://doi.org/10.1007/BF02846693

Kassis, A.I., 2004. The Amazing World of Auger Electrons. Int J Radiat Biol 80, 789–803. https://doi.org/10.1080/09553000400017663

Koning, A.J., Rochman, D., Sublet, J.C., Dzysiuk, N., Fleming, M., van der Marck, S., 2019. TENDL: Complete Nuclear Data Library for Innovative Nuclear Science and Technology. Nuclear Data Sheets 155, 1–55. https://doi.org/10.1016/j.nds.2019.01.002

Lahiri, S., Maiti, M., Ghosh, K., 2013. Production and separation of ^{111}In: an important radionuclide in life sciences: a mini review. J Radioanal Nucl Chem 297, 309–318. https://doi.org/10.1007/s10967-012-2344-3

Landini, L., Osso, J.A., 2001. Simultaneous Production of ^{57}Co and^{109}Cd in Cyclotron. J Radioanal Nucl Chem 250, 429–431. https://doi.org/10.1023/A:1017928501399

Lubberink, M., Tolmachev, V., Widstro, C., Bruskin, A., Lundqvist, H., Westlin, J., 2002. for Imaging of Neuroendocrine Tumors with PET. J.Nucl.med. 43, 1391–1397.

Mansur, M.S., Mushtaq, A., Muhammad, A., 1995. A109Cd/109mAg generator. J Radioanal Nucl Chem 201, 205–211. https://doi.org/10.1007/BF02164828

Mirzaii, M., Sadeghi, M., Gholamzadeh, Z., 2009. Targetry for cyclotron production of no-carrier-added cadmium-109 from ^{nat}Ag(p,n)^{109}Cd reaction. Iran. J. Radiat. Res. 6, 201–206.

Misri, R., Saatchi, K., Ng, S.S.W., Kumar, U., Häfeli, U.O., 2011. Evaluation of ^{111}In labeled antibodies for SPECT imaging of mesothelin expressing tumors. Nucl Med Biol 38, 885–896. https://doi.org/10.1016/J.NUCMEDBIO.2011.02.013

Mitterhauser, M., Wadsak, W., Key Mien, L.-, Eidherr, H., Roka, S., Zettinig, G., Angelberger, P., Viernstein, H., Kletter, K., Dudczak, R., 2003. The labelling of Nanocoll® with [111In] for dual-isotope scanning. Applied Radiation and Isotopes 59, 337–342. https://doi.org/10.1016/j.apradiso.2003.09.002

Mukhrjee, S., Mohan Rao, A. V, Rao, J.R., 1991. Pre-equilibrium analysis of the excitation functions of (α,xn) reactions on silver and holmium. Il Nuovo Cimento A (1991) 104, 863–874. https://doi.org/10.1007/BF02820560

National Nuclear Data Center, 2019. Nuclear structure and decay data on-line library, Nudat 2.8 [WWW Document]. URL http://www.nndc.bnl.gov/nudat2/

Otuka, N., Takács, S., 2015. Definitions of radioisotope thick target yields. Radiochim Acta 103, 1–6.

https://doi.org/10.1515/ract-2013-2234

Peng, X., Long, X., He, F., Liu, M., 1996. Excitation functions and yields of the reactions induced by alpha-particle bombardment of natural silver. Applied Radiation and Isotopes 47, 309–313. https://doi.org/10.1016/0969-8043(95)00276-6

Porges, K.G., 1956. Alpha Excitation Functions of Silver and Copper. Physical Review 101, 225–230. https://doi.org/10.1103/PhysRev.101.225

Pritychenko, B., Sonzogni, A., 2003. Q-value Calculator (QCalc) [WWW Document]. URL http://www.nndc.bnl.gov/qcalc/

Shahid, M., Kim, K., Kim, G., Naik, H., Zaman, M., Lee, Y.O., Cho, Y.S., 2017. Measurement of excitation functions of the natAg(α,x) reactions up to 45 MeV. J Radioanal Nucl Chem 311, 1971–1981. https://doi.org/10.1007/s10967-016-5122-9

Singh, N.L., Agarwal, S., Chaturvedi, L., Rao, J.R., 1987. Excitation functions for radioactive isotopes produced by alpha particle induced reactions with silver. Nucl Instrum Methods Phys Res B 24–25, 480–483. https://doi.org/https://doi.org/10.1016/0168-583X(87)90688-4

Sitarz, M., Cussonneau, J.P., Matulewicz, T., Haddad, F., 2020. Radionuclide candidates for β+γ coincidence PET: An overview. Applied Radiation and Isotopes 155, 108898. https://doi.org/10.1016/j.apradiso.2019.108898

Takács, S., Hermanne, A., Tárkányi, F., Ignatyuk, A., 2010. Cross-sections for alpha particle produced radionuclides on natural silver. Nucl Instrum Methods Phys Res B 268, 2–12. https://doi.org/10.1016/j.nimb.2009.09.035

Takács, S., Király, B., Tárkányi, F., Hermanne, A., 2007. Evaluated activation cross sections of longer-lived radionuclides produced by deuteron induced reactions on natural titanium. Nucl Instrum Methods Phys Res B 262, 7–12. https://doi.org/10.1016/j.nimb.2007.05.011

Tárkányi, F., Ditrói, F., Takács, S., Csikai, J., Hermanne, A., Uddin, M.S., Baba, M., 2018. Production routes of ^{107,109}Cd radioisotopes via charged particle induced nuclear reactions. J Radioanal Nucl Chem 318, 1949–1966. https://doi.org/10.1007/s10967-018-6226-1

Tárkányi, F., Takács, S., Ditrói, F., Hermanne, A., Baba, M., Mohsena, B.M.A., Ignatyuk, A. V, 2015. New cross section data and review of production routes of medically used ^{110m}In. Nucl Instrum Methods Phys Res B 351, 6–15. https://doi.org/https://doi.org/10.1016/j.nimb.2015.03.067

Thakur, M.L., 1977. Gallium-67 and indium-111 radiopharmaceuticals. Int J Appl Radiat Isot 28, 183–201. https://doi.org/10.1016/0020-708X(77)90172-7

Tolmachev, V., Stone-Elander, S., 2010. Radiolabelled proteins for positron emission tomography: Pros and cons of labelling methods. Biochim Biophys Acta Gen Subj 1800, 487–510. https://doi.org/10.1016/j.bbagen.2010.02.002

Verpelli, M., Abriola, D., 2011. Information management tools for evaluated nuclear structure data file (ENSDF) interrogation and dissemination. Journal of the Korean Physical Society 59, 1322–1324.

https://doi.org/10.3938/jkps.59.1322

Wasilevsky, C., de la Vega Vedoya, M., Nassiff, S.J., 1985a. Excitation functions for (α,xn) reactions on ^{107}Ag and ^{109}Ag. J Radioanal Nucl Chem 89, 531–543. https://doi.org/10.1007/BF02040616

Wasilevsky, C., De la Vega Vedoya, M., Nassiff, S.J., 1985b. Isomer yield ratios and cross sections for $^{110(4.9\ h)}$In/$^{110(69\ min)}$In and $^{108(58min)}$In/$^{108(39.6\ min)}$In produced by alpha reactions on silver. J Radioanal Nucl Chem 95, 29–44. https://doi.org/10.1007/BF02166241

Wasilevsky, C., Ozafran, M.J., de la Vega Vedoya, M., Nassiff, S.J., 1988. (α,αxn) and (α,2pxn) reactions on ^{107}Ag and ^{109}Ag. J Radioanal Nucl Chem 121, 115–129. https://doi.org/10.1007/BF02041453

Watanabe, T., Fujimaki, M., Fukunishi, N., Imao, H., Kamigaito, O., Kase, M., Komiyama, M., Sakamoto, N., Suda, K., Wakasugi, M., Yamada, K., 2014. Beam energy and longitudinal beam profile measurement system at the RIBF, in: Proceedings of the 5th International Particle Accelerator Conference (IPAC 2014). pp. 3566–3568.

Ziegler, J.F., Ziegler, M.D., Biersack, J.P., 2010. SRIM - The stopping and range of ions in matter (2010). Nucl Instrum Methods Phys Res B 268, 1818–1823. https://doi.org/10.1016/j.nimb.2010.02.091

Figure captions

Fig. 1. The excitation function of the ^{nat}Ti(α,x)^{51}Cr monitor reaction compared with the recommended values (Hermanne et al., 2018; Takács et al., 2007).

Fig. 2. Excitation function of the ^{nat}Ag(α,x)^{111g}In reaction.

Fig. 3. Excitation function of the ^{nat}Ag(α,x)^{110m}In reaction.

Fig. 4. Excitation function of the ^{nat}Ag(α,x)^{110g}In reaction.

Fig. 5. Excitation function of the ^{nat}Ag(α,x)^{109g}In reaction.

Fig. 6. Excitation function of the ^{nat}Ag(α,x)^{108m}In reaction.

Fig. 7. Excitation function of the ^{nat}Ag(α,x)^{108g}In reaction.

Fig. 8. Excitation function of the ^{nat}Ag(α,x)^{107g}In reaction.

Fig. 9. Excitation function of the ^{109}Ag(α,x)^{111m}Cd reaction.

Fig. 10. Excitation function of the $^{nat}Ag(\alpha,x)^{109}Cd$ reaction.

Fig. 11. Excitation function of the $^{nat}Ag(\alpha,x)^{107}Cd$ reaction.

Fig. 12. Excitation function of the $^{nat}Ag(\alpha,x)^{110m}Ag$ reaction.

Fig. 13. Excitation function of the $^{nat}Ag(\alpha,x)^{106m}Ag$ reaction.

Fig. 14. Excitation function of the $^{nat}Ag(\alpha,x)^{105g}Ag$ reaction.

Fig. 15. Excitation function of the $^{nat}Ag(\alpha,x)^{104g}Ag$ reaction.

Fig. 16. The physical yield of ^{111}In produced by the (α,x) reaction on ^{nat}Ag.

Fig. 17. The physical yields of $^{110m,110g}In$ produced by the (α,x) reactions on ^{nat}Ag.

Fig. 18. The physical yield of ^{109}Cd produced by the (α,x) reactions on ^{nat}Ag.

Table 1

Reactions and decay data for the investigated reaction products (International Atomic Energy Agency, 2009; National Nuclear Data Center, 2019; Pritychenko and Sonzogni, 2003). γ lines in bold were used in our evaluation.

Nuclide	Half-life	Decay mode (%)	E_γ (keV)	I_γ (%)	Contributing reaction channels	Q-value (MeV)	Threshold energy (MeV)
^{111}In	2.8047 d	ε (100)	**171.28**	**90.7(9)**	^{109}Ag(α,2n)	-14.05	14.45
			245.35	94.1(10)	^{107}Ag(α,γ)	2.40	0.00
^{110m}In	69.1 min	ε+β$^+$ (100)	511.0	122.5(8)	^{109}Ag(α,3n)	-24.04	24.74
			657.75	**97.74(7)**	^{107}Ag(α,n)	-7.58	7.81
^{110g}In	4.9 h	ε+β$^+$ (100)	641.68	26.0(8)	^{109}Ag(α,3n)	-24.04	24.74
			657.75	98(3)	^{107}Ag(α,n)	-7.58	7.81
			707.40	29.5(11)			
			884.667	**93(3)**			
			937.478	68.4(19)			
			997.16	10.5(3)			
^{109}In	4.167 h	ε (100)	**203.3**	**74.2(5)**	^{109}Ag(α,4n)	-32.09	33.03
					^{107}Ag(α,2n)	-15.64	16.10
^{108m}In	39.6 min	ε+β$^+$ (100)	511.0	100.8(23)	^{109}Ag(α,5n)	-42.53	43.77
			632.9	**76.4(6)**	^{107}Ag(α,3n)	-26.08	26.85
			1986.3	12.4(7)			
^{108g}In	58.0 min	ε+β$^+$ (100)	242.6	41(5)	^{109}Ag(α,5n)	-42.53	43.77
			325.6	13.7(15)	^{107}Ag(α,3n)	-26.08	26.85
			511.0	50(3)			
			632.9	100(7)			
			875.4	100(11)			
			1032.8	**35(3)**			
			1056.6	29(3)			
			1299.3	15.1(16)			
^{107}In	32.4 min	ε+β$^+$ (100)	**204.95**	**47.2(3)**	^{107}Ag(α,4n)	-34.70	35.74
			320.94	10.2(3)			
			505.51	11.9(4)			
			511.0	72(6)			
^{111m}Cd	48.50 min	IT (100)	**150.825**	**29.1(18)**	^{109}Ag(α,np)	-12.40	12.76
					^{109}Ag(α,d)	-10.18	10.48
			245.395	94(7)	Decay of ^{111g}In		
					Decay of ^{111g}Ag		
^{109}Cd	461.9 d	ε (100)	**88.0336**	**3.644(16)**	^{109}Ag(α,3np)	-29.29	30.15
					^{109}Ag(α,2nd)	-27.01	27.86
					^{109}Ag(α,nt)	-20.81	21.42
					^{107}Ag(α,np)	-12.84	13.22
					^{107}Ag(α,d)	-10.61	10.93
					Decay of ^{109g}In		
^{107}Cd	6.5 h	ε (100)	**93.124**	**4.7(3)**	^{109}Ag(α,5np)	-46.95	48.32
					^{109}Ag(α,4nd)	-44.73	46.03
					^{109}Ag(α,3nt)	-38.47	39.59
					^{107}Ag(α,3np)	-30.49	31.41
					^{107}Ag(α,2nd)	-28.27	29.11
					^{107}Ag(α,nt)	-22.01	22.67

^{110m}Ag	249.83 d	β^- (98.64)	**657.76**	**95.61(9)**	^{109}Ag(α,n2p)	-21.49	22.11
		IT (1.36)	677.6217	10.70(5)	^{109}Ag(α,pd)	-19.26	19.82
			706.6760	16.69(7)	^{109}Ag(α,^{3}He)	-13.77	14.17
			763.9424	22.60(7)			
			884.6781	75.0(11)			
			937.485	35.0(3)			
			1384.2931	25.1(5)			
			1505.0280	13.33(15)			
^{106m}Ag	8.28 d	ε (100)	221.701	6.6(3)	^{109}Ag(α,4n^{3}He)	-46.57	47.93
			406.182	13.4(4)	^{109}Ag(α,3npt)	-45.81	47.14
			429.646	13.2(4)	^{109}Ag(α,2ndt)	-43.58	44.85
			450.976	**28.2(7)**	^{109}Ag(α,n2t)	-37.32	38.41
			511.85	88(8)	^{109}Ag(α,3nα)	-25.99	26.75
			616.17	21.6(6)	^{107}Ag(α,3n2p)	-37.83	38.96
			717.34	28.9(8)	^{107}Ag(α,2npd)	-35.60	36.67
			748.36	20.6(6)	^{107}Ag(α,n2d)	-33.38	34.38
			824.69	15.3(4)	^{107}Ag(α,2n^{3}He)	-30.11	31.01
			1045.83	29.6(10)	^{107}Ag(α,npt)	-29.35	30.23
			1128.02	11.8(5)	^{107}Ag(α,dt)	-27.13	27.94
			1199.39	11.2(5)	^{107}Ag(α,nα)	-9.54	9.82
			1527.65	16.3(13)			
^{105}Ag	41.29 d	ε+β^+ (100)	64.072	11.3(11)	^{109}Ag(α,2n2t)	-45.27	46.59
			280.54	**31(3)**	^{109}Ag(α,4nα)	-33.93	34.92
			344.52	42(4)	^{107}Ag(α,4n2p)	-45.77	47.14
			443.37	10.9(10)	^{107}Ag(α,3npd)	-43.55	44.85
			644.55	10.2(10)	^{107}Ag(α,2n2d)	-41.33	42.56
					^{107}Ag(α,3n^{3}He)	-38.06	39.19
					^{107}Ag(α,2npt)	-37.29	38.41
					^{107}Ag(α,ndt)	-35.07	36.12
					^{107}Ag(α,2t)	-28.81	29.67
					^{107}Ag(α,2nα)	-17.48	18.00
					Decay of ^{105}Cd		
^{104g}Ag	69.2 min	ε+β^+ (100)	555.8	92.6	^{109}Ag(α,5nα)	-43.96	45.24
			767.6	**65.7**	^{107}Ag(α,4n^{3}He)	-48.08	49.52
			857.9	10.4	^{107}Ag(α,3npt)	-47.32	48.73
			941.6	25	^{107}Ag(α,2ndt)	-45.09	46.44
			1341.8	7.3	^{107}Ag(α,n2t)	-38.84	40.00
					^{107}Ag(α,3nα)	-27.50	28.33
^{51}Cr	27.704 d	ε (100)	**320.0824**	**9.910(10)**	^{50}Ti(α,3n)	-21.77	23.35
					^{49}Ti(α,2n)	-10.83	11.64
					^{48}Ti(α,n)	-2.68	2.89
					^{47}Ti(α,γ)	8.93	0.00

Table 2

Production cross sections derived in the experiment. The midpoint projectile energy, total uncertainty, and energy loss of each foil are shown in the first column.

Energy (MeV)	Cross sections (mb)						
	^{111}In	^{110m}In	^{110g}In	^{109}In	^{108m}In	^{108g}In	^{107g}In
49.1 ± 0.2 ± 0.4	27.4 ± 1.9	10.6 ± 0.9	172 ± 14	412 ± 30	51.6 ± 8.5	123 ± 17	170 ± 13
48.3 ± 0.2 ± 0.4	28.5 ± 2.1	11.0 ± 0.9	189 ± 15	394 ± 29	65.8 ± 9.1	147 ± 20	154 ± 12
46.4 ± 0.2 ± 0.4	32.8 ± 2.4	17.8 ± 1.4	242 ± 20	345 ± 25	59.0 ± 10.9	171 ± 23	114 ± 10
45.6 ± 0.2 ± 0.4	31.4 ± 2.3	23.8 ± 1.9	279 ± 22	318 ± 23	72.4 ± 11.8	186 ± 25	94.5 ± 8.3
43.6 ± 0.2 ± 0.4	36.8 ± 2.7	25.5 ± 1.9	355 ± 28	252 ± 19	92.5 ± 14.1	214 ± 29	51.9 ± 5.8
42.7 ± 0.2 ± 0.4	45.6 ± 3.3	37.2 ± 2.9	379 ± 30	228 ± 17	89.7 ± 14.9	227 ± 30	37.1 ± 4.8
40.7 ± 0.3 ± 0.5	58.2 ± 4.2	54.7 ± 4.2	442 ± 35	169 ± 13	123 ± 17	237 ± 32	
39.8 ± 0.3 ± 0.5	57.3 ± 4.2	60.9 ± 4.7	455 ± 36	148 ± 11	125 ± 18	230 ± 31	
37.6 ± 0.3 ± 0.5	90.8 ± 6.6	83.0 ± 6.3	464 ± 37	160 ± 12	109 ± 17	216 ± 29	
36.6 ± 0.3 ± 0.5	108 ± 8	82.8 ± 6.3	460 ± 37	180 ± 13	124 ± 18	207 ± 28	
34.3 ± 0.3 ± 0.5	173 ± 13	93.3 ± 7.2	400 ± 32	278 ± 20	86.9 ± 15.7	149 ± 21	
33.3 ± 0.3 ± 0.5	212 ± 15	87.6 ± 6.8	372 ± 30	342 ± 25	105 ± 16	116 ± 16	
30.8 ± 0.4 ± 0.6	353 ± 26	76.5 ± 6.2	228 ± 18	487 ± 35	49.6 ± 9.9	38.8 ± 6.2	
29.7 ± 0.4 ± 0.6	424 ± 31	60.5 ± 4.9	164 ± 13	539 ± 39	18.5 ± 7.1	27.3 ± 4.6	
27.0 ± 0.4 ± 0.6	565 ± 41	19.7 ± 2.1	47.4 ± 4.2	573 ± 42			
25.8 ± 0.5 ± 0.6	578 ± 42	7.90 ± 0.99	27.4 ± 2.7	554 ± 40			
22.8 ± 0.5 ± 0.7	517 ± 38	19.4 ± 2.1	47.2 ± 4.7	468 ± 34			
21.4 ± 0.6 ± 0.7	458 ± 33	21.4 ± 2.1	75.8 ± 6.5	340 ± 28			
18.0 ± 0.7 ± 0.8	246 ± 18	103 ± 9	133 ± 11	129 ± 10			
16.4 ± 0.7 ± 0.9	123 ± 9	139 ± 12	94.8 ± 7.9	33.9 ± 2.8			
12.2 ± 0.9 ± 1.1	0.251 ± 0.019	24.9 ± 5.5	5.14 ± 0.76				
10.0 ± 1.1 ± 1.3	0.0341 ± 0.0026	2.24 ± 0.30	0.282 ± 0.030				
Energy (MeV)	Cross sections (mb)						
	^{111m}Cd	^{109}Cd	^{107}Cd	^{110m}Ag	^{106m}Ag	^{105}Ag	^{104}Ag
49.1 ± 0.2 ± 0.4	15.7 ± 2.9	537 ± 42	340 ± 34	2.86 ± 0.49	35.4 ± 2.8	69.5 ± 8.4	18.5 ± 2.5
48.3 ± 0.2 ± 0.4	14.3 ± 2.8	523 ± 38	302 ± 30	2.25 ± 0.19	32.5 ± 2.6	69.9 ± 8.4	14.7 ± 2.2
46.4 ± 0.2 ± 0.4	17.2 ± 3.4	453 ± 36	224 ± 23	2.10 ± 0.29	23.7 ± 1.9	70.2 ± 8.5	5.28 ± 1.78
45.6 ± 0.2 ± 0.4	15.3 ± 3.5	438 ± 35	181 ± 19	1.71 ± 0.41	21.3 ± 1.7	68.0 ± 8.3	
43.6 ± 0.2 ± 0.4	17.7 ± 3.8	369 ± 30	107 ± 13	1.24 ± 0.23	19.4 ± 1.6	61.7 ± 7.5	
42.7 ± 0.2 ± 0.4	19.4 ± 3.9	298 ± 25	65.6 ± 9.8	0.706 ± 0.201	19.4 ± 1.6	56.8 ± 6.9	
40.7 ± 0.3 ± 0.5	21.9 ± 4.4	228 ± 19	23.7 ± 8.9	0.616 ± 0.200	22.4 ± 1.8	46.1 ± 5.6	
39.8 ± 0.3 ± 0.5	21.9 ± 4.9	221 ± 20		0.616 ± 0.203	23.7 ± 1.9	38.9 ± 4.7	
37.6 ± 0.3 ± 0.5	28.1 ± 4.9	227 ± 20			28.0 ± 2.2	23.8 ± 2.9	
36.6 ± 0.3 ± 0.5	29.1 ± 4.9	267 ± 23			30.3 ± 2.4	18.4 ± 2.3	
34.3 ± 0.3 ± 0.5	31.9 ± 5.4	384 ± 31			30.9 ± 2.9	7.33 ± 0.94	
33.3 ± 0.3 ± 0.5	35.4 ± 5.5	445 ± 35			30.4 ± 3.2	4.00 ± 0.54	
30.8 ± 0.4 ± 0.6	32.5 ± 5.1	614 ± 47			18.3 ± 1.9	0.596 ± 0.172	
29.7 ± 0.4 ± 0.6	26.4 ± 6.3	652 ± 50			16.5 ± 1.8		
27.0 ± 0.4 ± 0.6	20.5 ± 3.8	676 ± 52			8.98 ± 1.40		
25.8 ± 0.5 ± 0.6	16.2 ± 4.1	619 ± 47			7.96 ± 1.27		
22.8 ± 0.5 ± 0.7	8.15 ± 3.35	521 ± 39			1.86 ± 0.28		
21.4 ± 0.6 ± 0.7		416 ± 31					
18.0 ± 0.7 ± 0.8		143 ± 12					
16.4 ± 0.7 ± 0.9		35.3 ± 4.1					

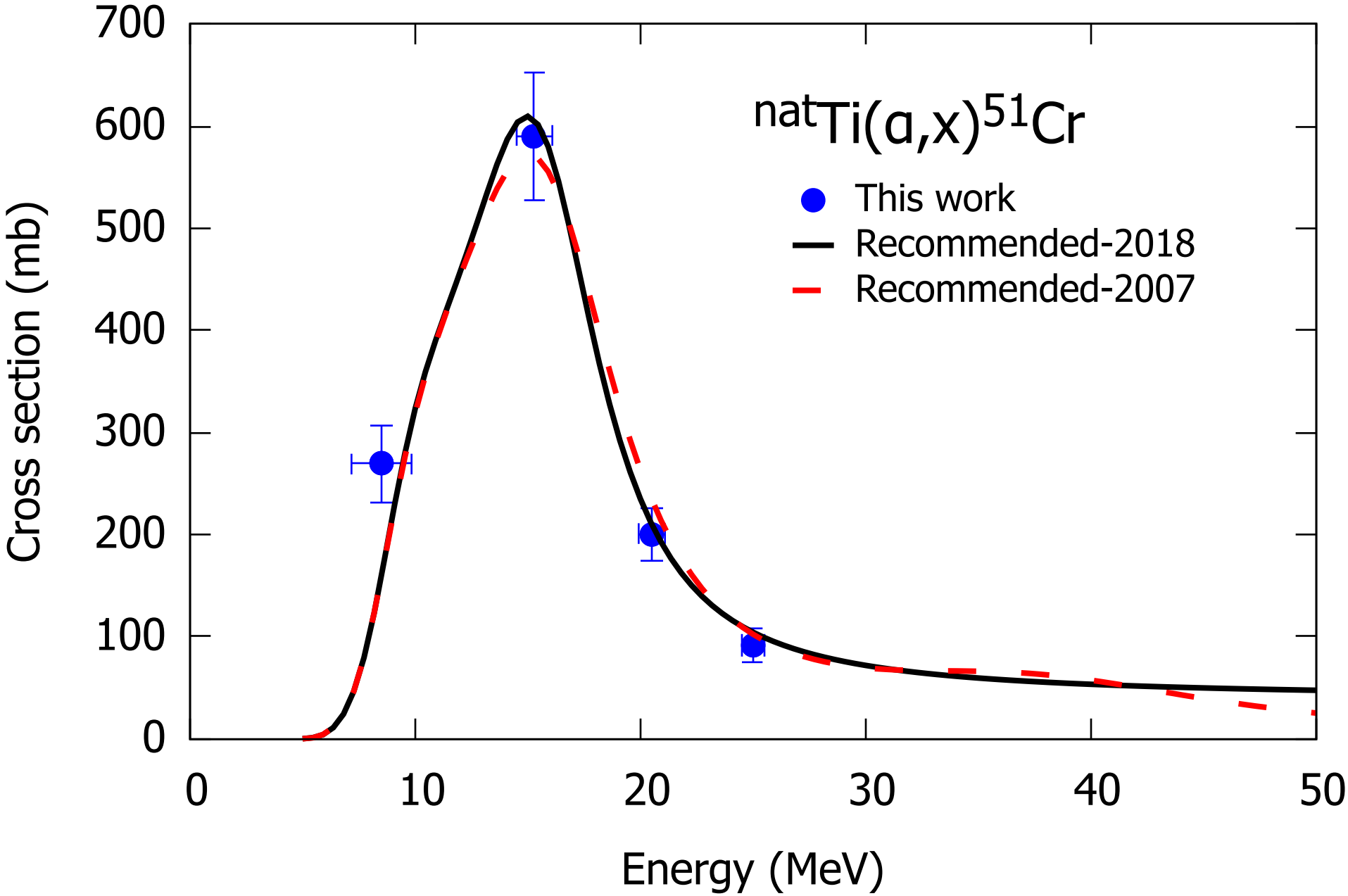
$^{nat}Ti(a,x)^{51}Cr$
This work
Recommended-2018
Recommended-2007
Cross section (mb)
Energy (MeV)
0
100
200
300
400
500
600
700
0
10
20
30
40
50

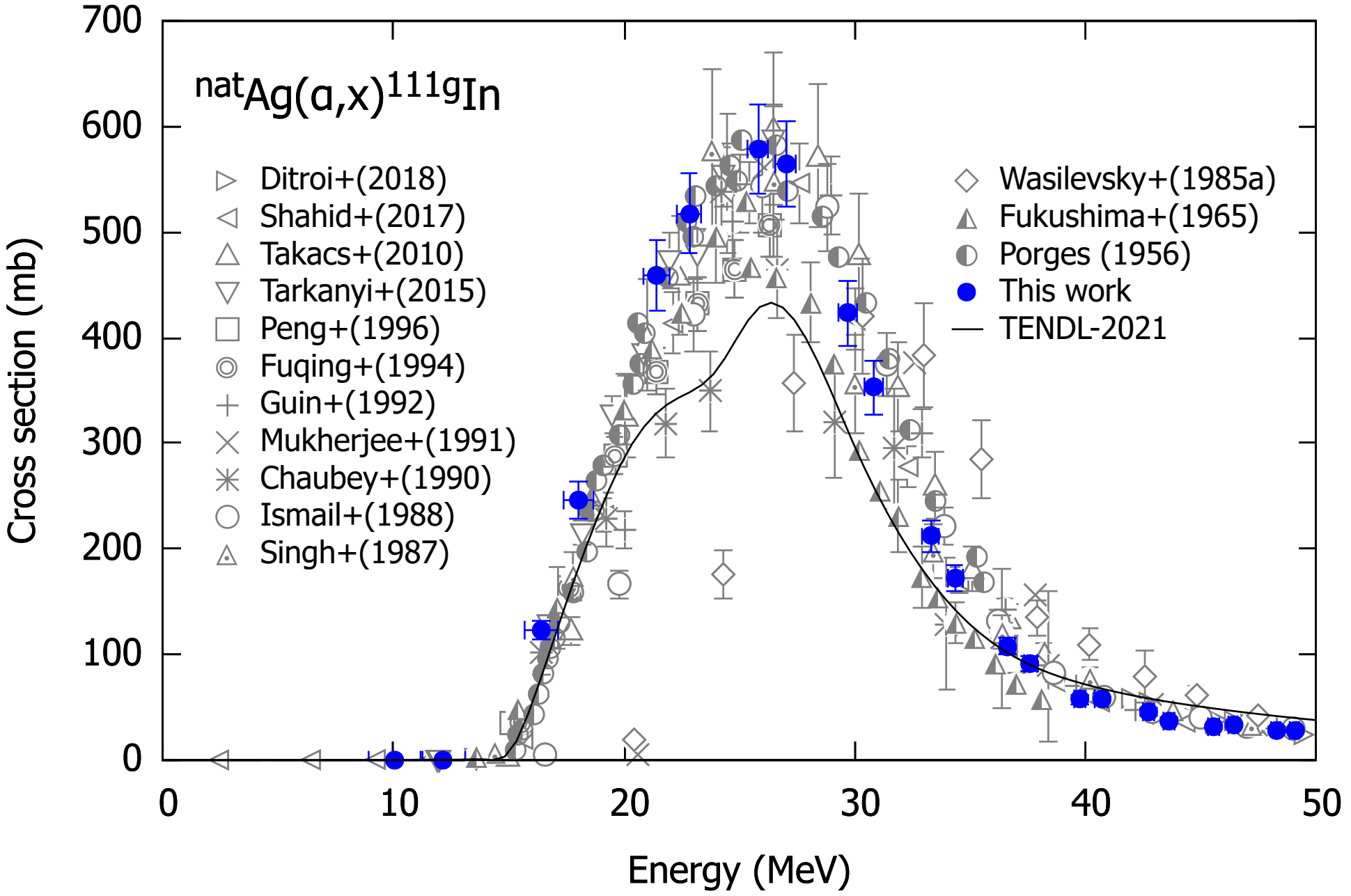
natAg(α,x)111gIn
Ditroi+(2018)
Shahid+(2017)
Takacs+(2010)
Tarkanyi+(2015)
Peng+(1996)
Fuqing+(1994)
Guin+(1992)
Mukherjee+(1991)
Chaubey+(1990)
Ismail+(1988)
Singh+(1987)
Wasilevsky+(1985a)
Fukushima+(1965)
Porges (1956)
This work
TENDL-2021
Cross section (mb)
Energy (MeV)
0
100
200
300
400
500
600
700
0
10
20
30
40
50

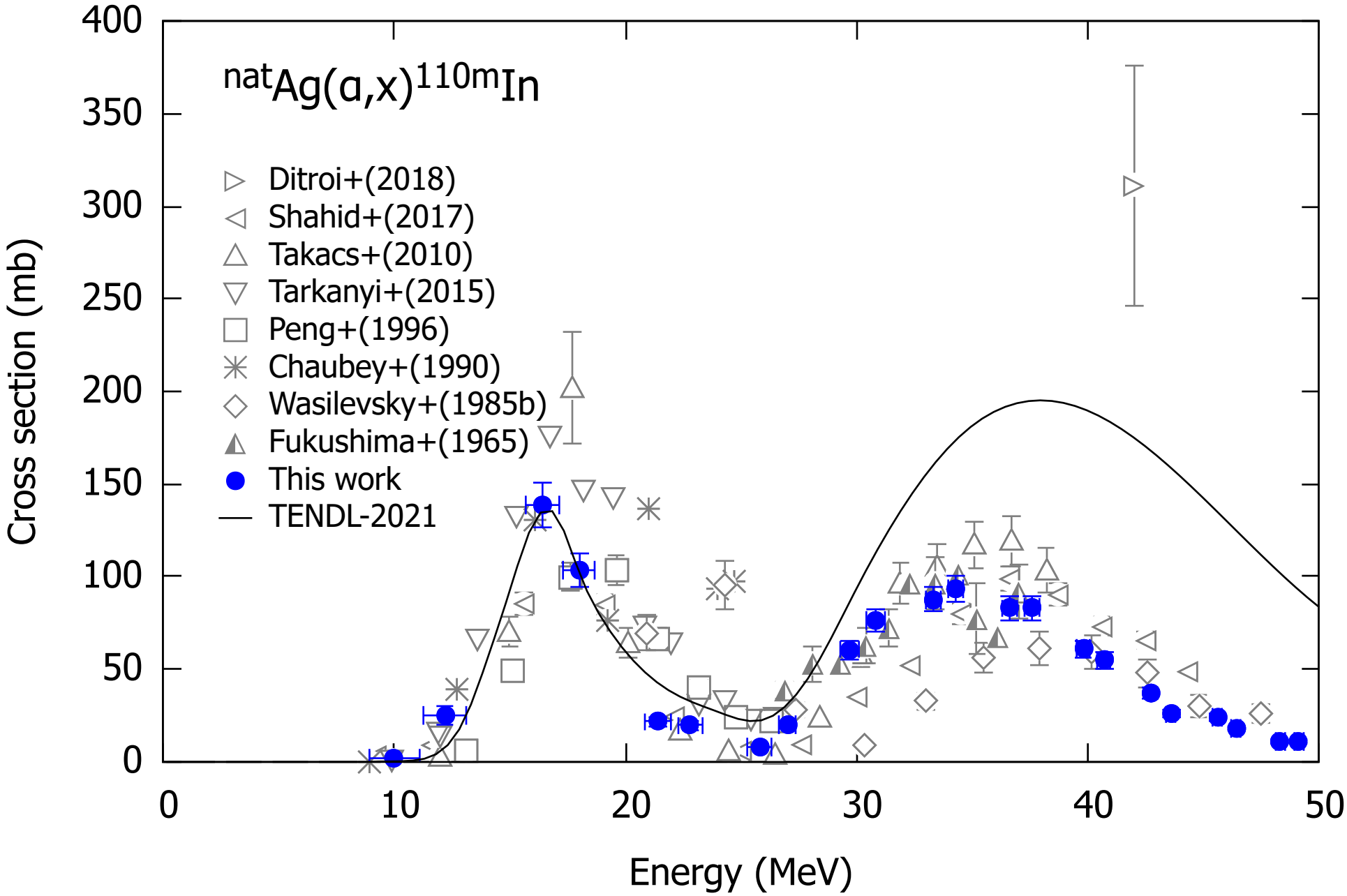
$^{nat}Ag(\alpha,x)^{110m}In$
Ditroi+(2018)
Shahid+(2017)
Takacs+(2010)
Tarkanyi+(2015)
Peng+(1996)
Chaubey+(1990)
Wasilevsky+(1985b)
Fukushima+(1965)
This work
TENDL-2021
Cross section (mb)
Energy (MeV)
0
50
100
150
200
250
300
350
400
0
10
20
30
40
50

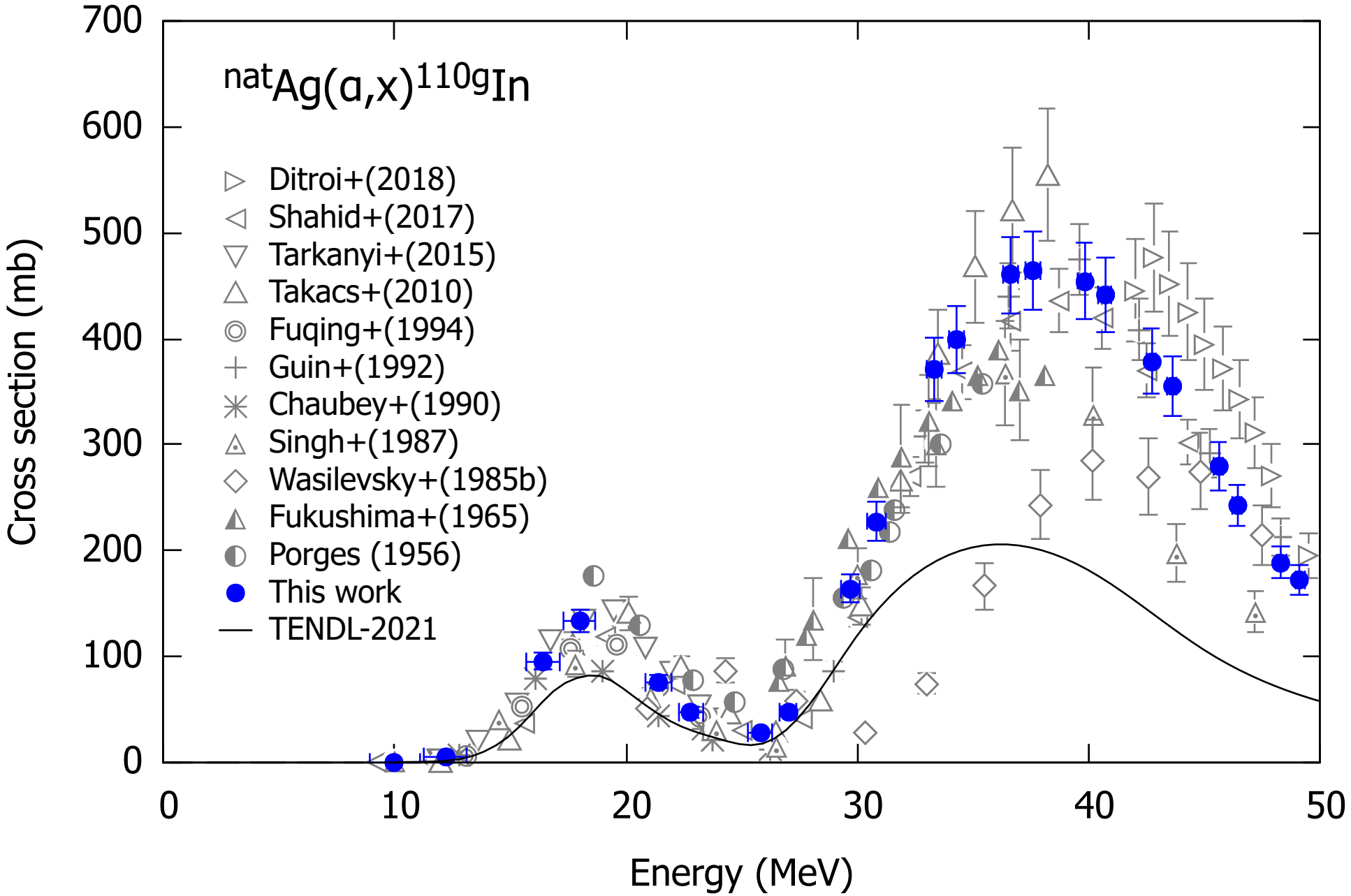
natAg(α,x)110gIn
Ditroi+(2018)
Shahid+(2017)
Tarkanyi+(2015)
Takacs+(2010)
Fuqing+(1994)
Guin+(1992)
Chaubey+(1990)
Singh+(1987)
Wasilevsky+(1985b)
Fukushima+(1965)
Porges (1956)
This work
TENDL-2021
Cross section (mb)
Energy (MeV)
0
100
200
300
400
500
600
700
0
10
20
30
40
50

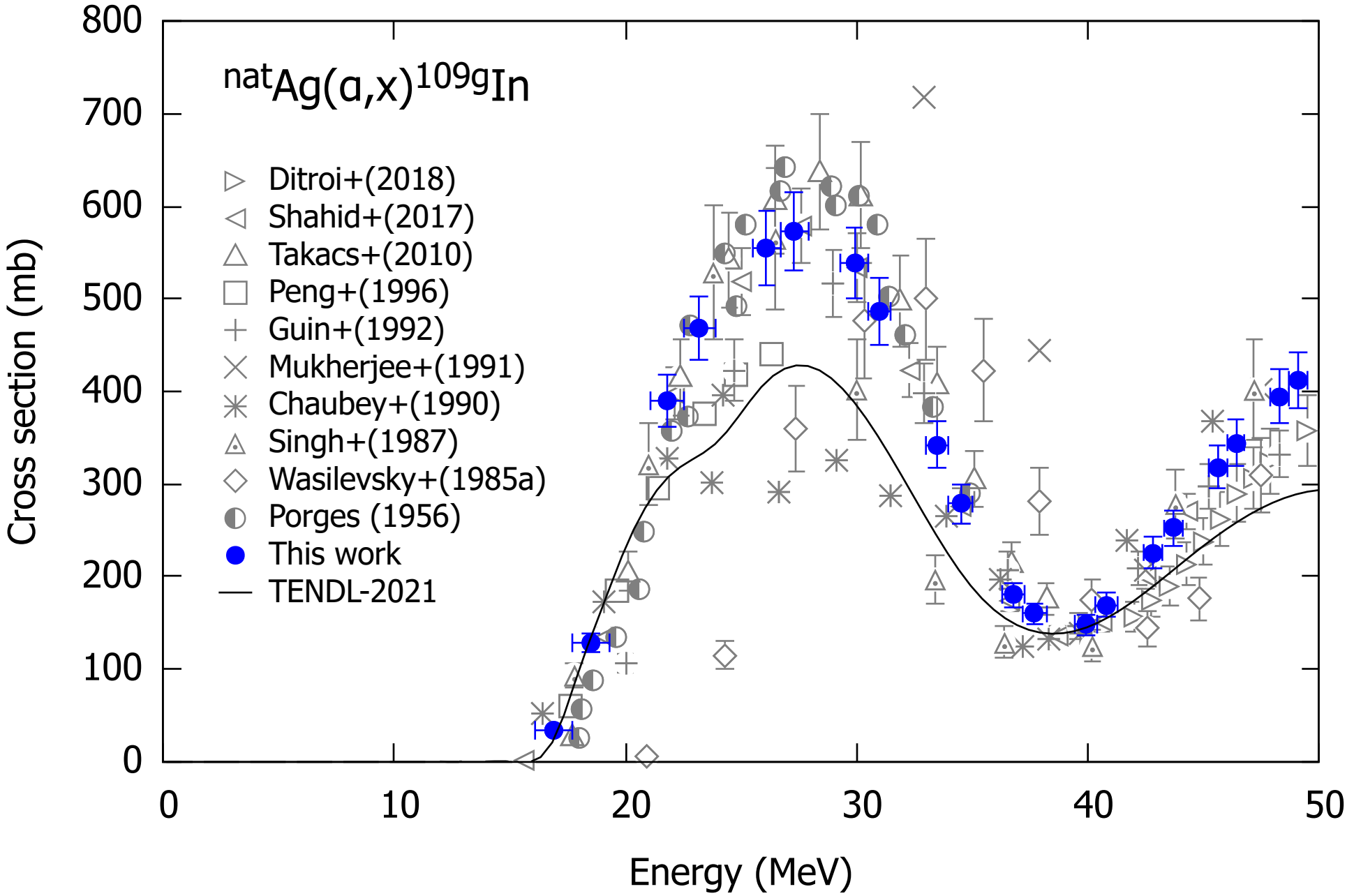
$^{nat}Ag(\alpha,x)^{109g}In$
Ditroi+(2018)
Shahid+(2017)
Takacs+(2010)
Peng+(1996)
Guin+(1992)
Mukherjee+(1991)
Chaubey+(1990)
Singh+(1987)
Wasilevsky+(1985a)
Porges (1956)
This work
TENDL-2021
Cross section (mb)
Energy (MeV)
0
100
200
300
400
500
600
700
800
0
10
20
30
40
50

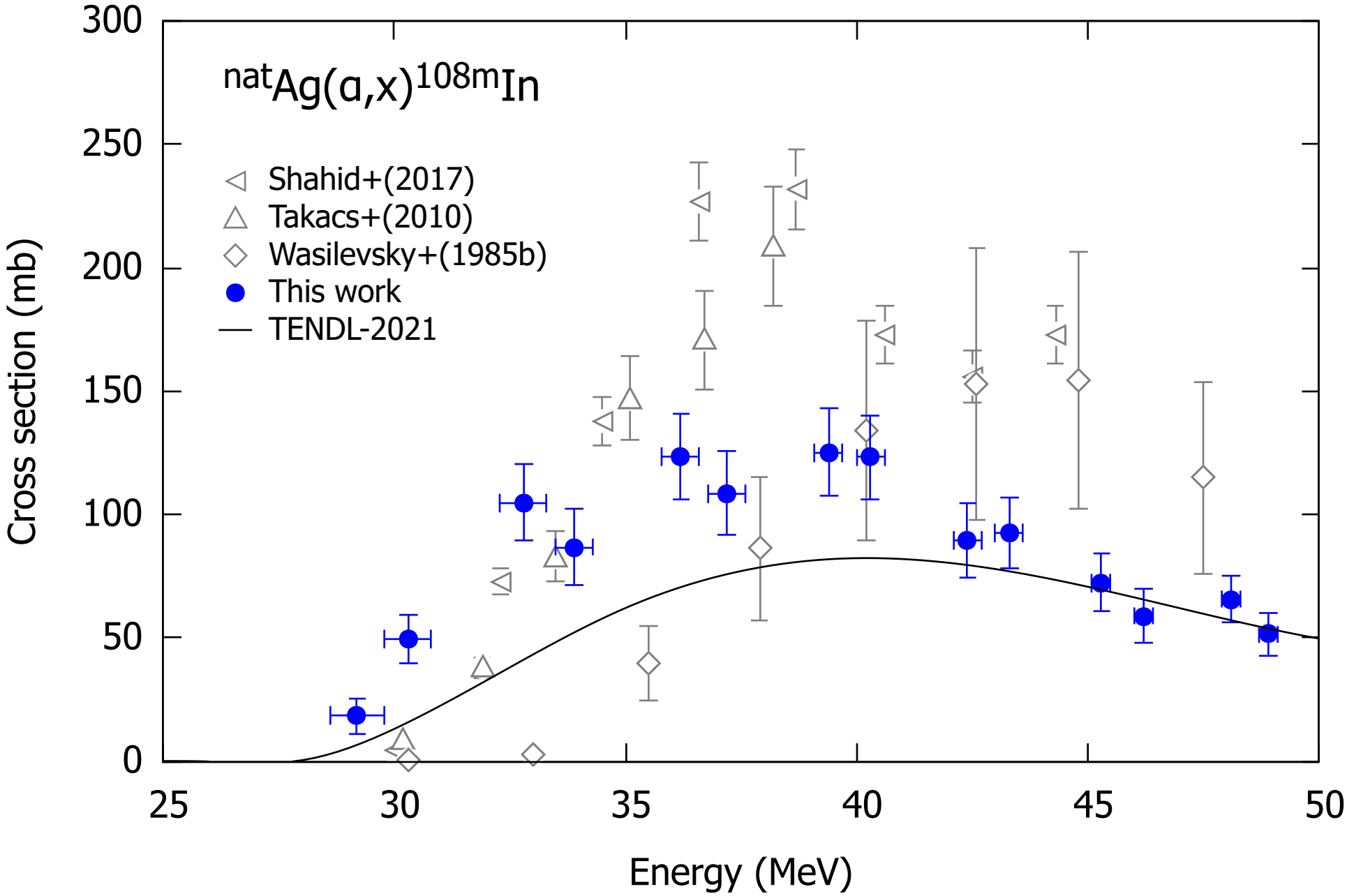
$^{nat}Ag(\alpha,x)^{108m}In$
Shahid+(2017)
Takacs+(2010)
Wasilevsky+(1985b)
This work
TENDL-2021
Cross section (mb)
Energy (MeV)
300
250
200
150
100
50
0
25
30
35
40
45
50

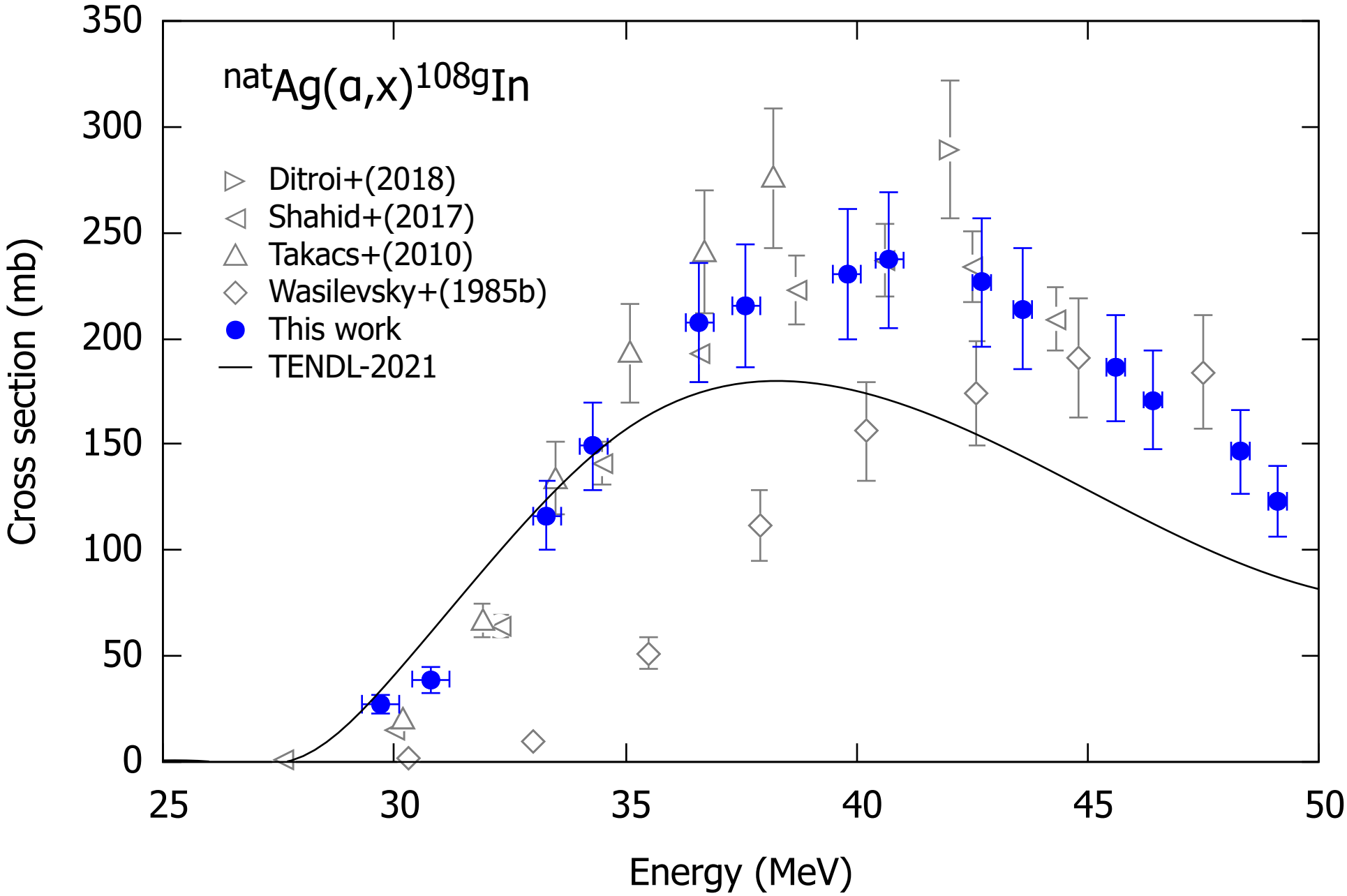
$^{nat}Ag(\alpha,x)^{108g}In$
Ditroi+(2018)
Shahid+(2017)
Takacs+(2010)
Wasilevsky+(1985b)
This work
TENDL-2021
Cross section (mb)
Energy (MeV)
0
50
100
150
200
250
300
350
25
30
35
40
45
50

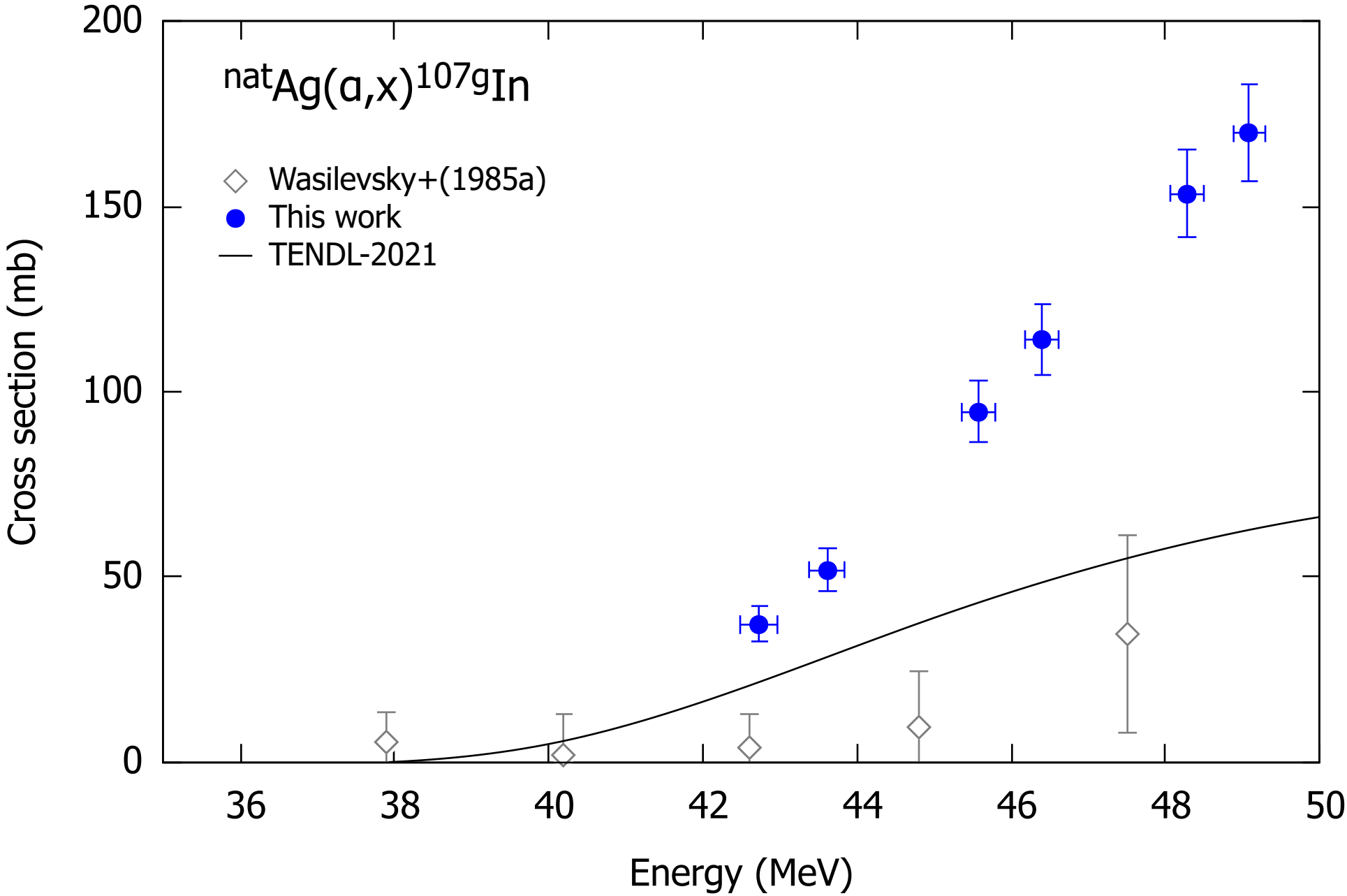
natAg(α,x)107gIn
Wasilevsky+(1985a)
This work
TENDL-2021
Cross section (mb)
Energy (MeV)
0
50
100
150
200
36
38
40
42
44
46
48
50

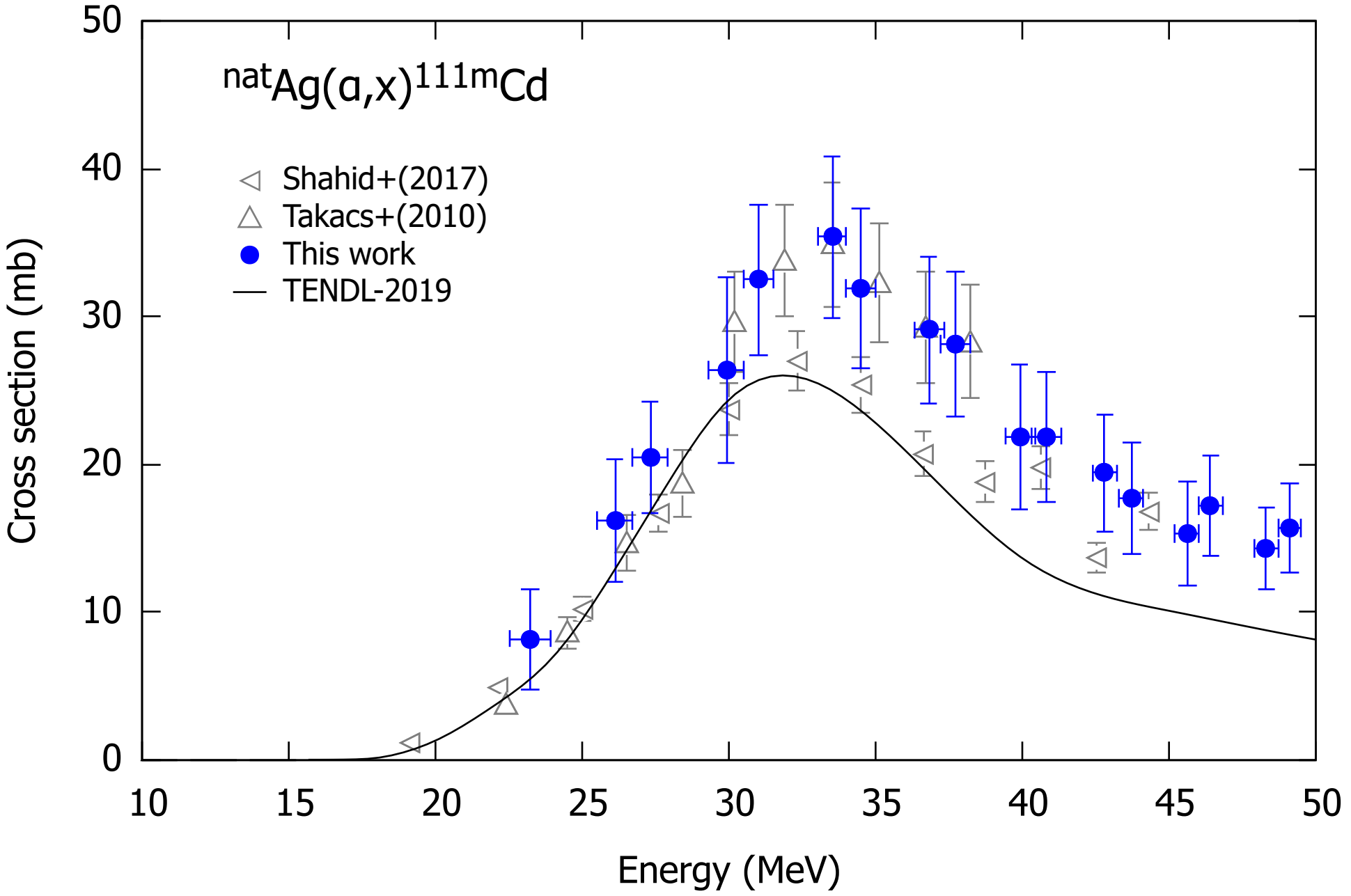
$^{nat}Ag(\alpha,x)^{111m}Cd$
Shahid+(2017)
Takacs+(2010)
This work
TENDL-2019
Cross section (mb)
Energy (MeV)
0
10
20
30
40
50
10
15
20
25
30
35
40
45
50

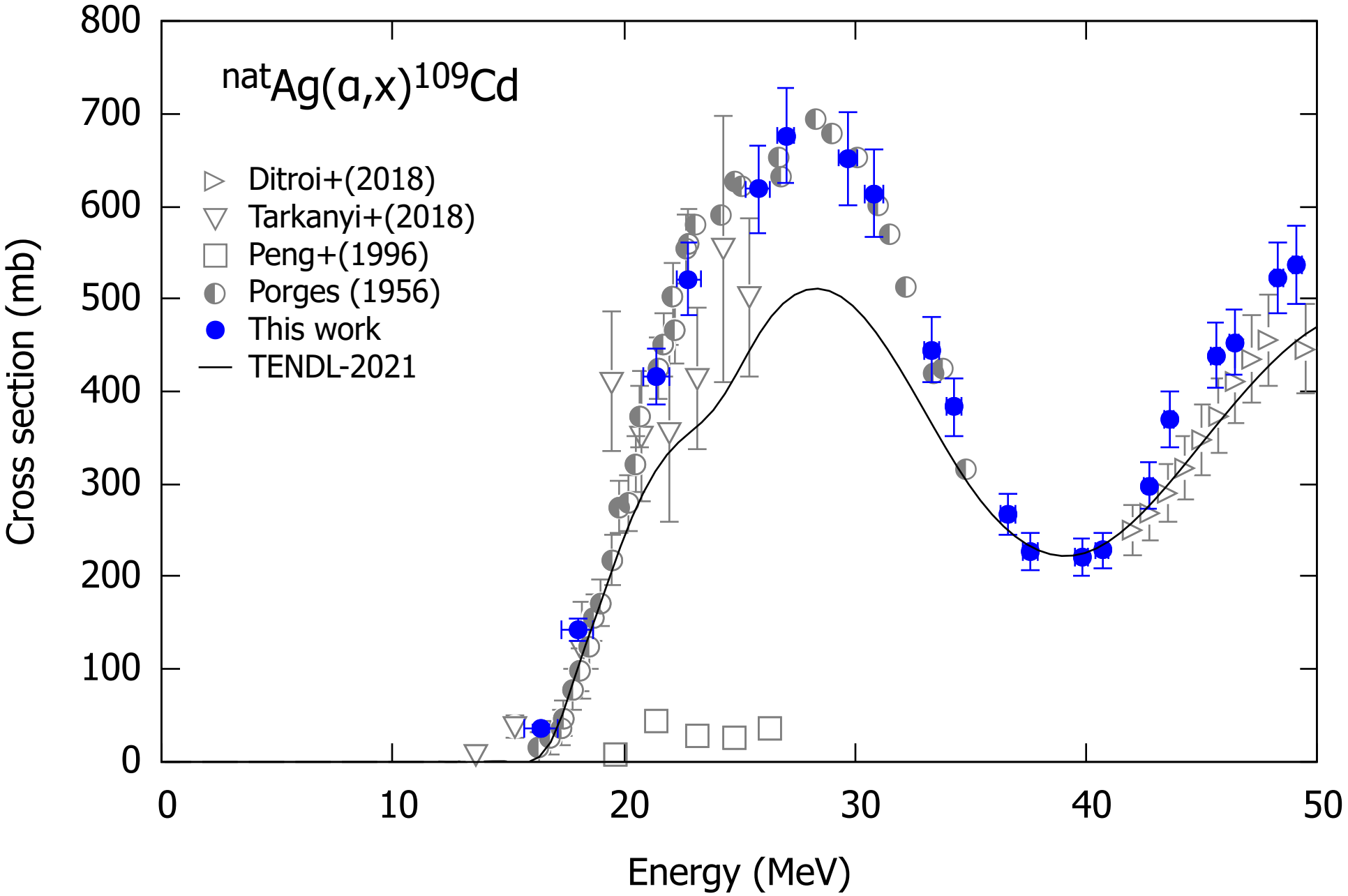
$^{nat}Ag(\alpha,x)^{109}Cd$
Ditroi+(2018)
Tarkanyi+(2018)
Peng+(1996)
Porges (1956)
This work
TENDL-2021
Cross section (mb)
Energy (MeV)
0
100
200
300
400
500
600
700
800
0
10
20
30
40
50

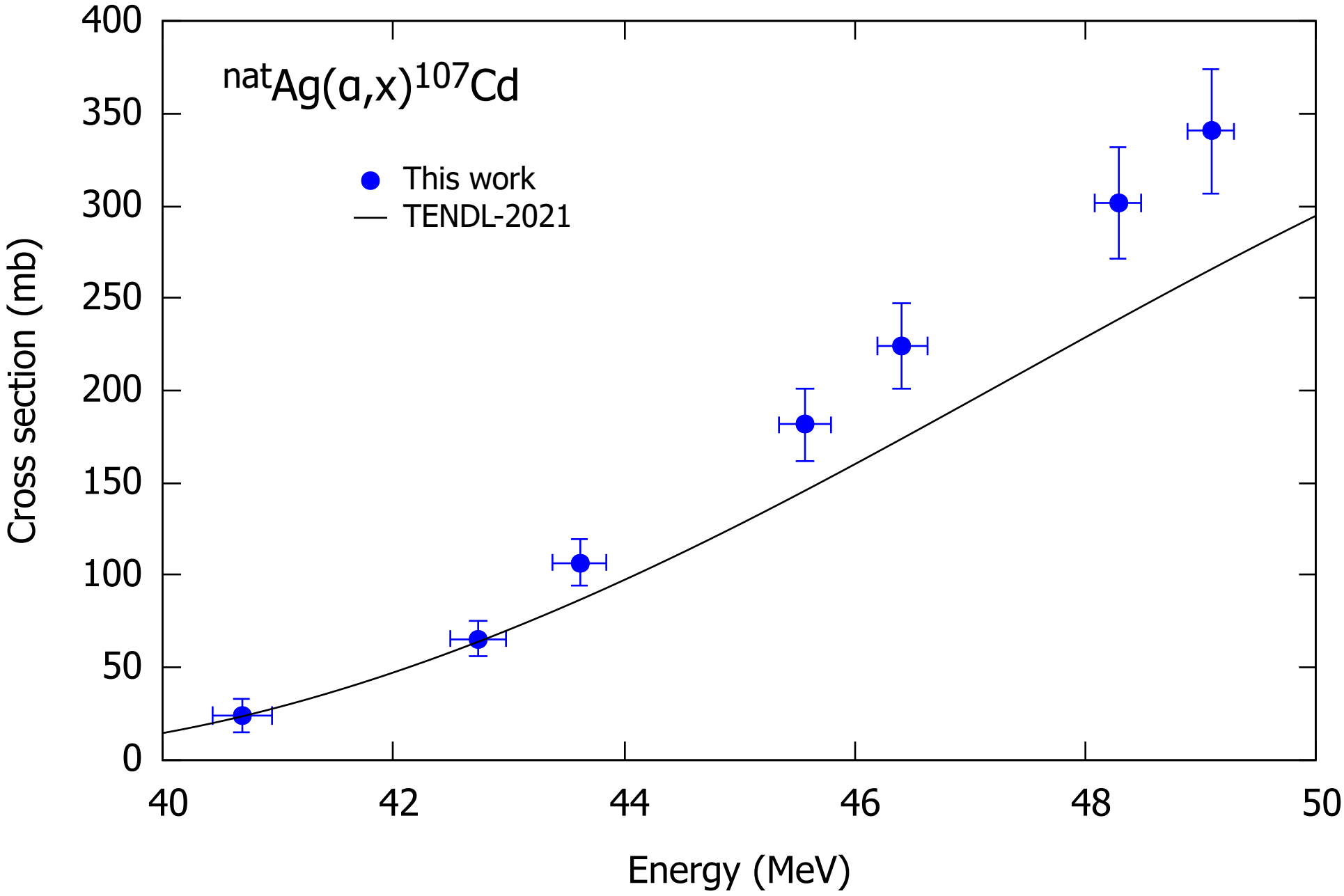
$^{nat}Ag(\alpha,x)^{107}Cd$
This work
TENDL-2021
Cross section (mb)
Energy (MeV)
0
50
100
150
200
250
300
350
400
40
42
44
46
48
50

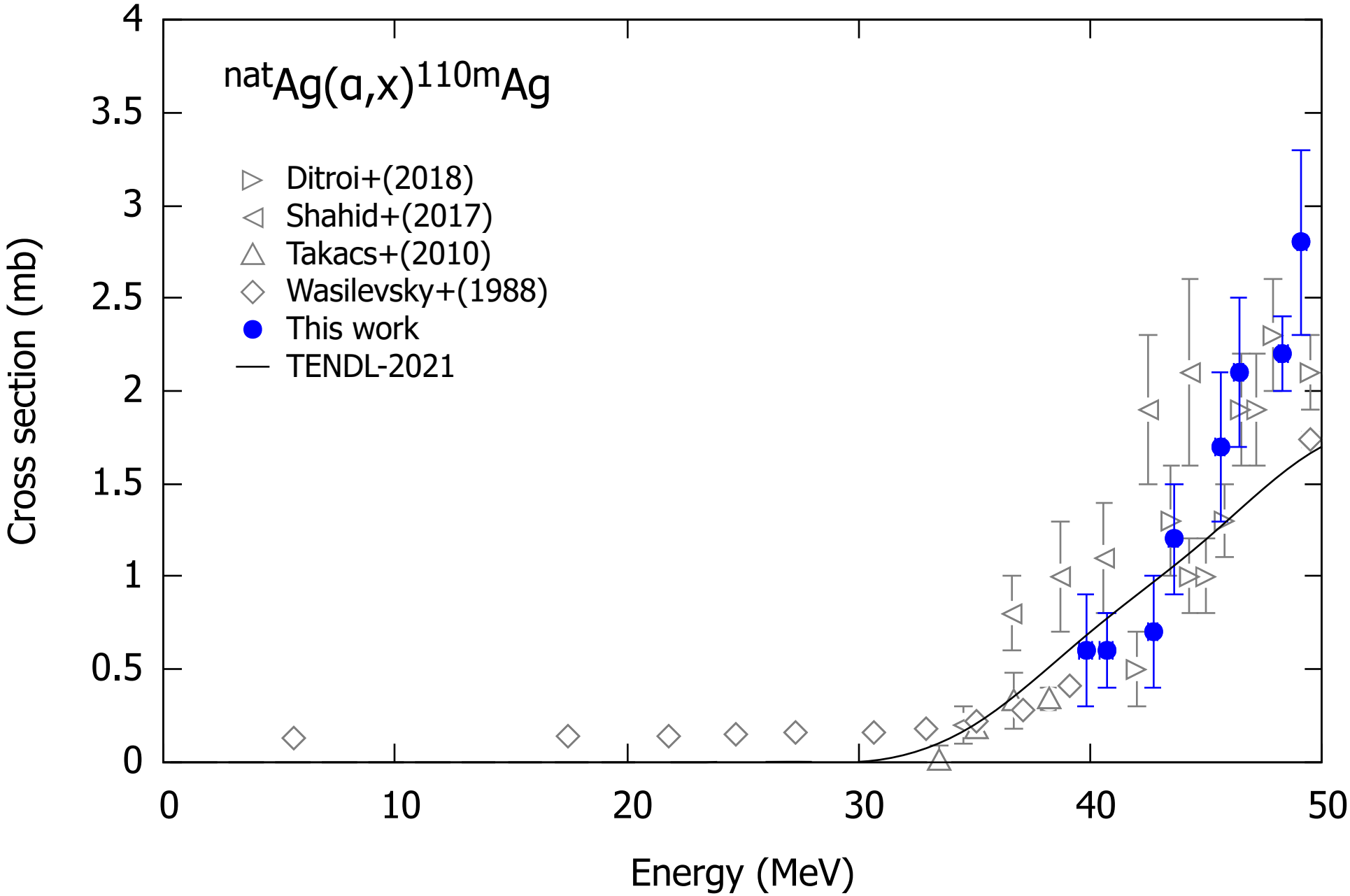
$^{nat}Ag(\alpha,x)^{110m}Ag$
Ditroi+(2018)
Shahid+(2017)
Takacs+(2010)
Wasilevsky+(1988)
This work
TENDL-2021
Cross section (mb)
Energy (MeV)
0
0.5
1
1.5
2
2.5
3
3.5
4
0
10
20
30
40
50

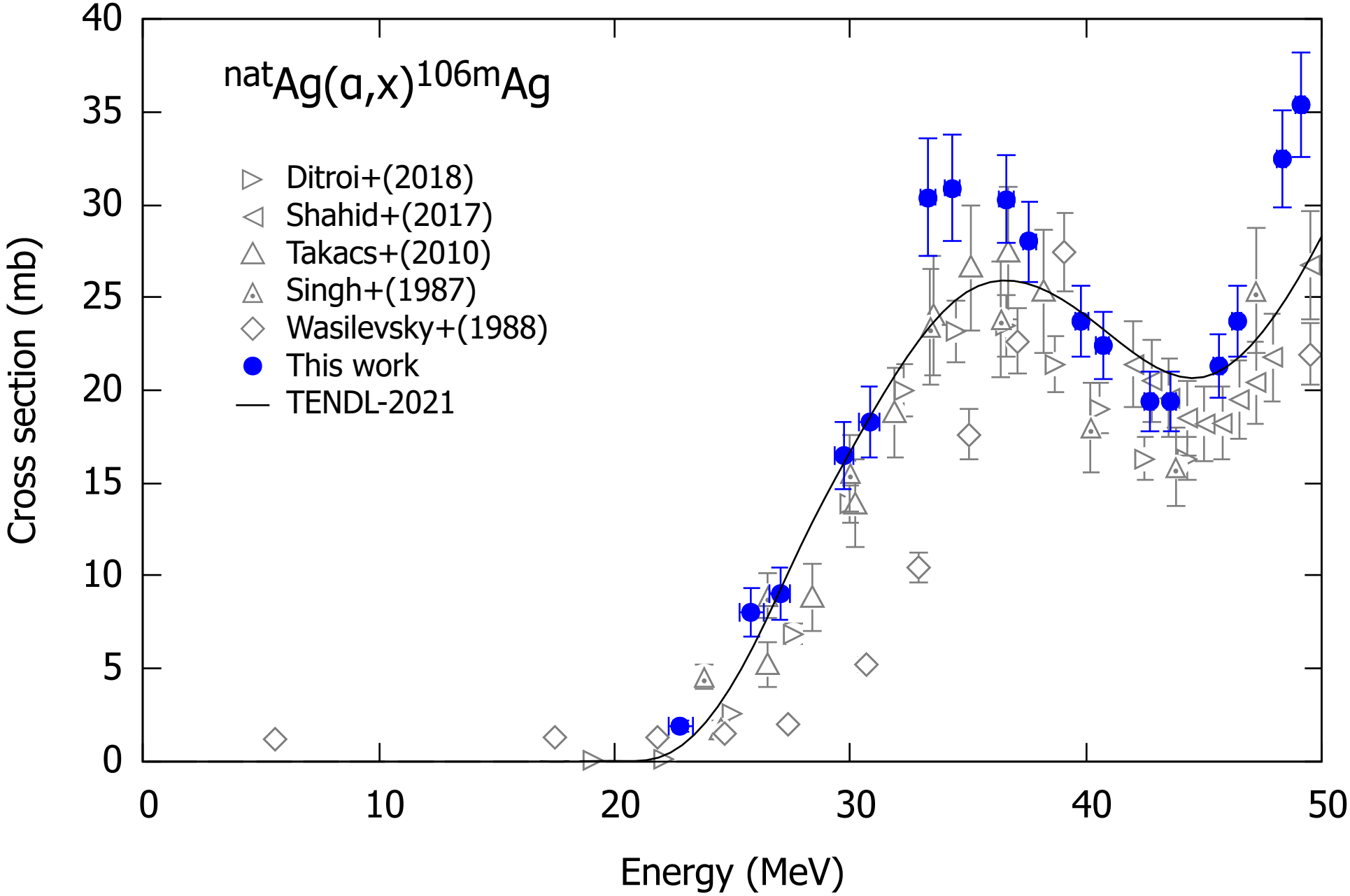
$^{nat}Ag(\alpha,x)^{106m}Ag$
Ditroi+(2018)
Shahid+(2017)
Takacs+(2010)
Singh+(1987)
Wasilevsky+(1988)
This work
TENDL-2021
Cross section (mb)
Energy (MeV)
0
5
10
15
20
25
30
35
40
0
10
20
30
40
50

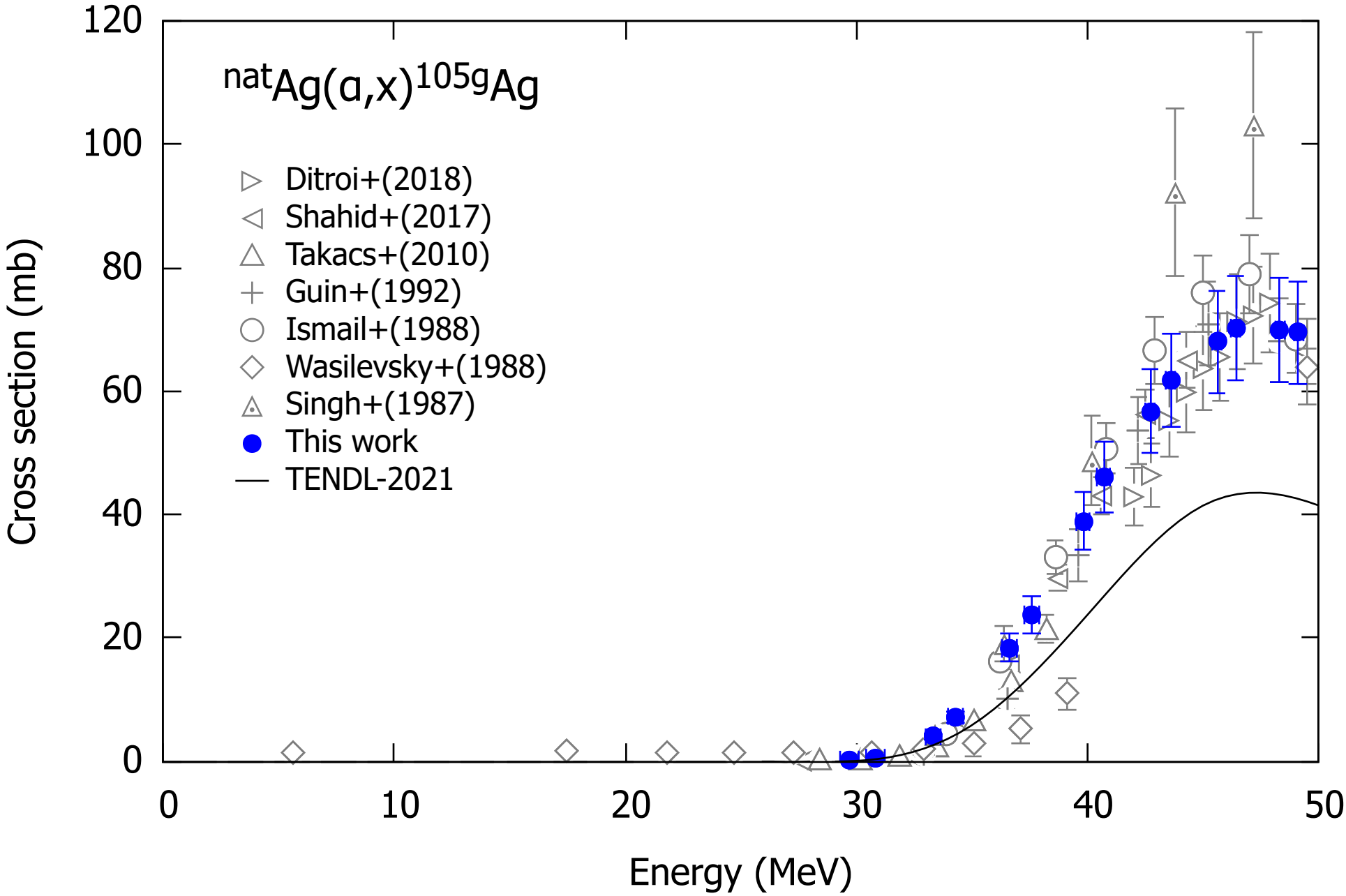
$^{nat}Ag(\alpha,x)^{105g}Ag$
Ditroi+(2018)
Shahid+(2017)
Takacs+(2010)
Guin+(1992)
Ismail+(1988)
Wasilevsky+(1988)
Singh+(1987)
This work
TENDL-2021
Cross section (mb)
Energy (MeV)
0
20
40
60
80
100
120
0
10
20
30
40
50

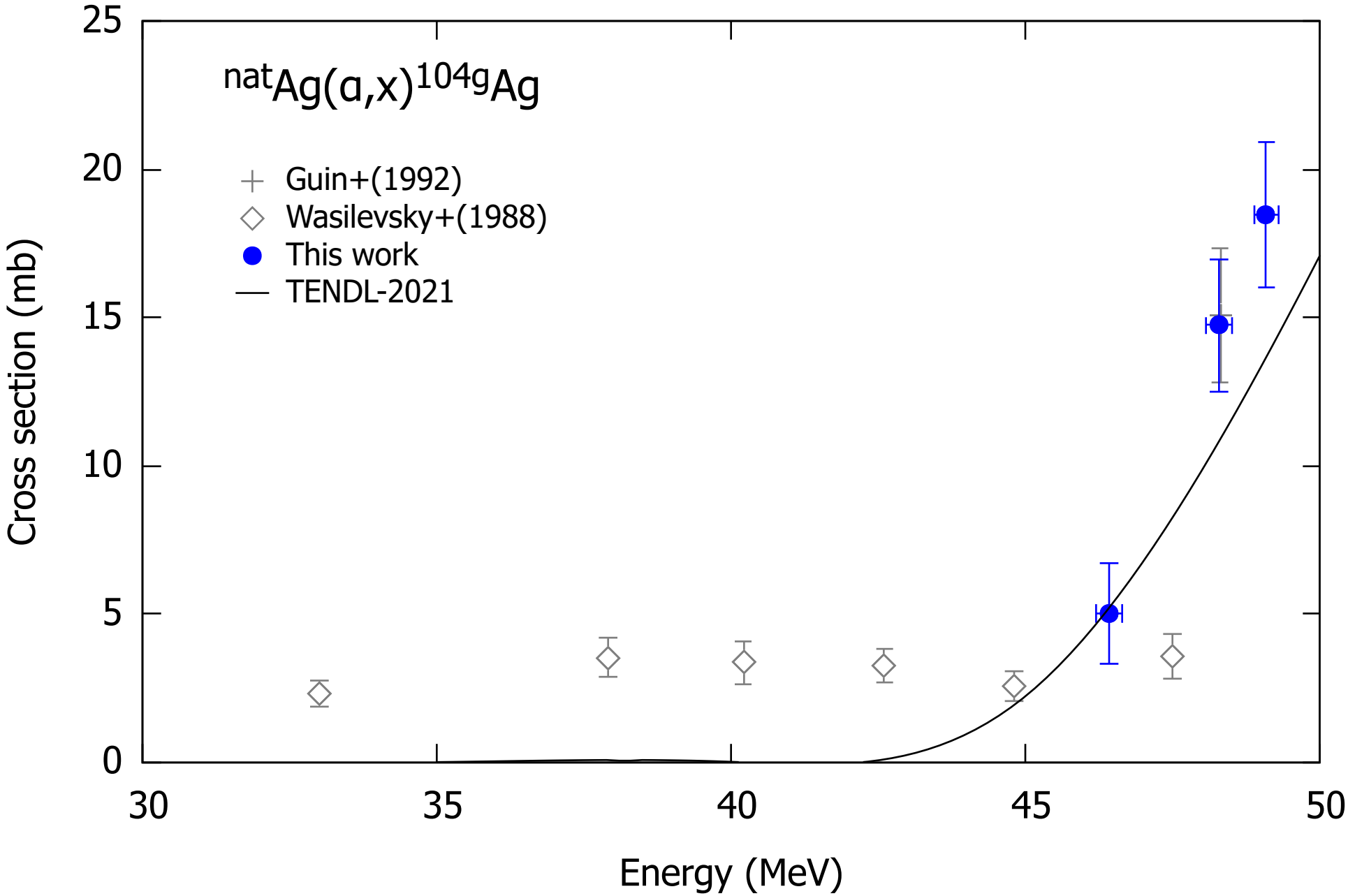
natAg(α,x)104gAg
Guin+(1992)
Wasilevsky+(1988)
This work
TENDL-2021
Cross section (mb)
Energy (MeV)
0
5
10
15
20
25
30
35
40
45
50

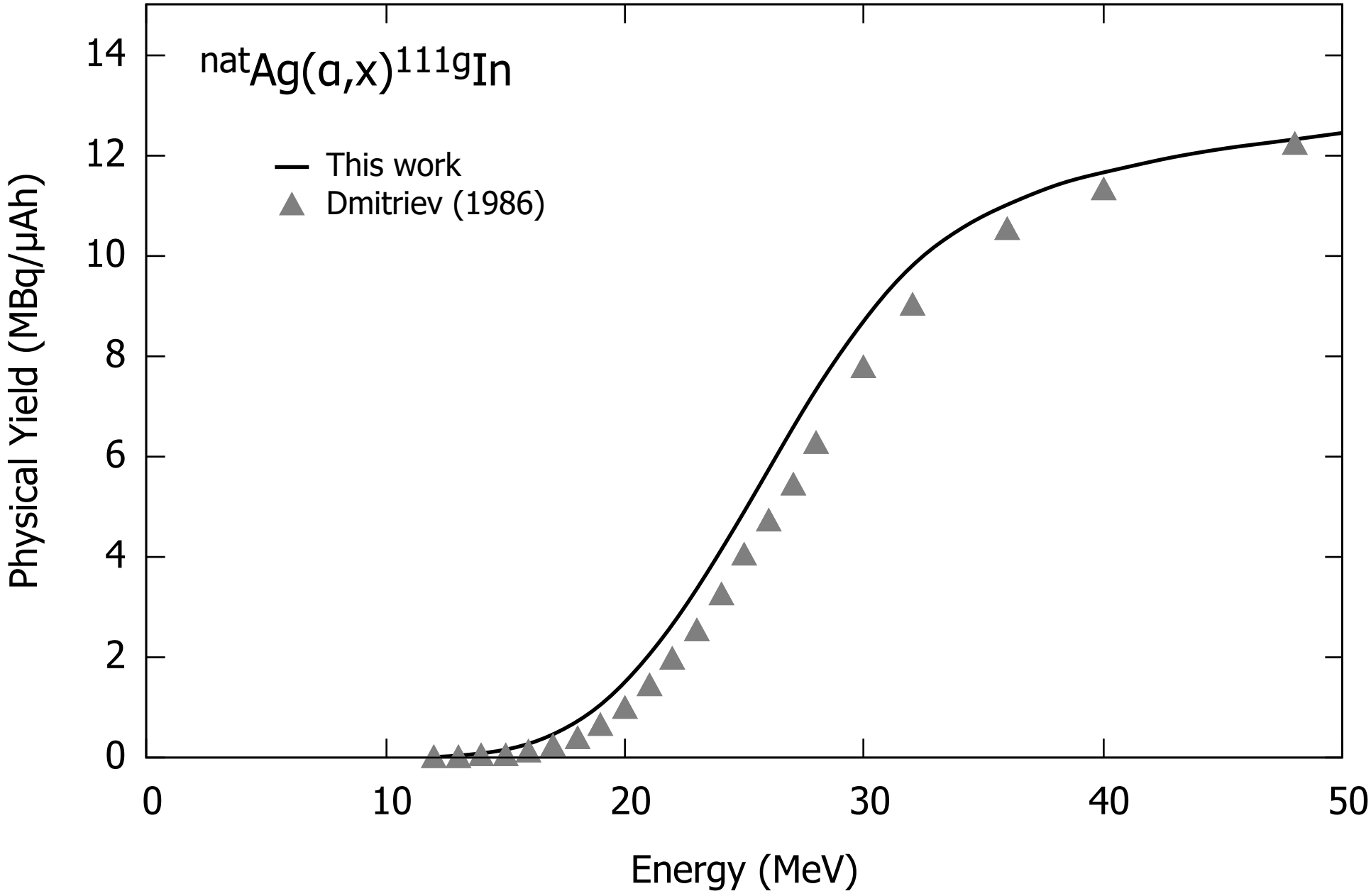
$^{nat}Ag(\alpha,x)^{111g}In$
This work
Dmitriev (1986)
Physical Yield (MBq/μAh)
Energy (MeV)
0
2
4
6
8
10
12
14
0
10
20
30
40
50

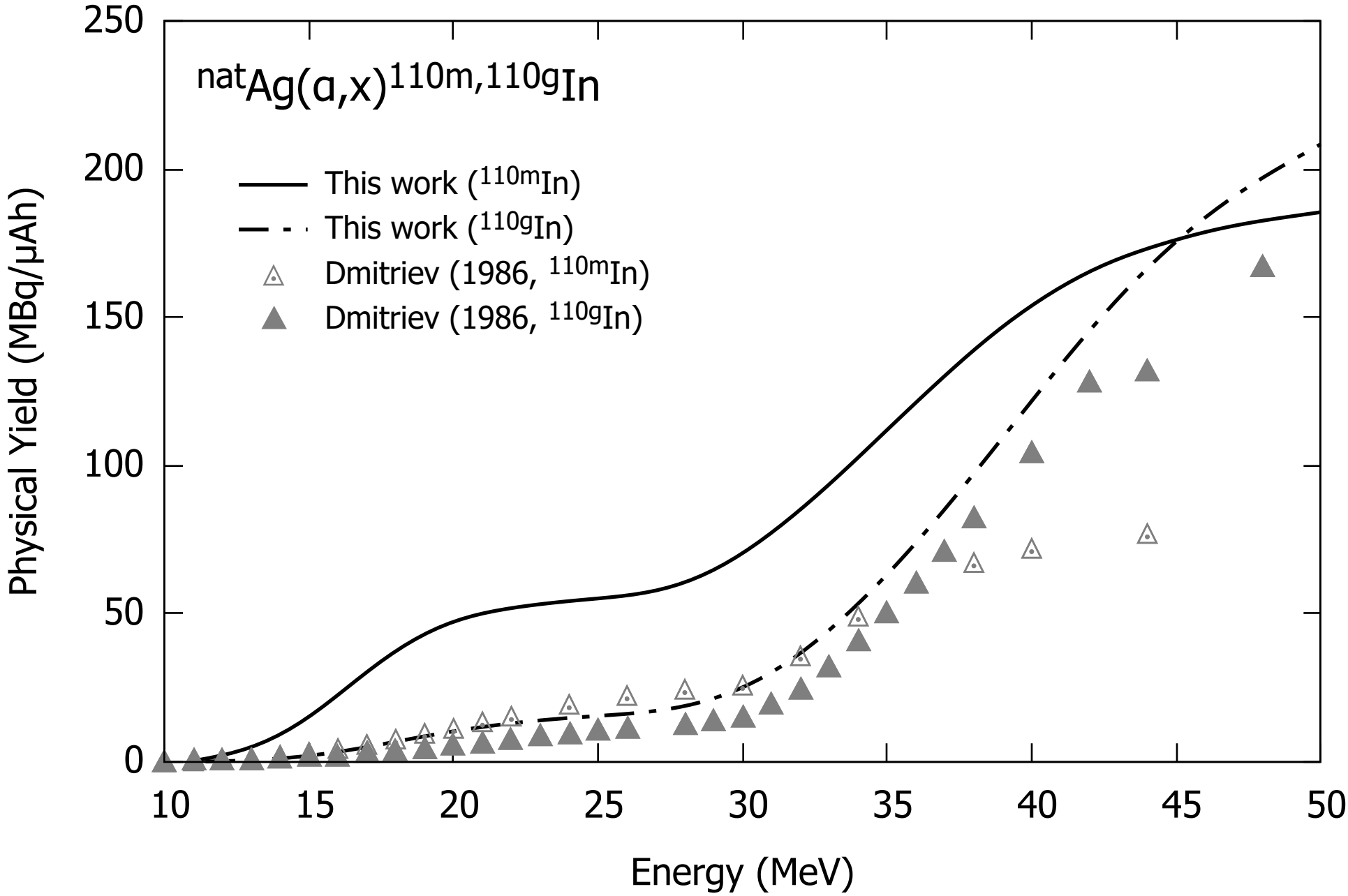
$^{nat}Ag(\alpha,x)^{110m,110g}In$
This work (^{110m}In)
This work (^{110g}In)
Dmitriev (1986, ^{110m}In)
Dmitriev (1986, ^{110g}In)
Physical Yield (MBq/μAh)
Energy (MeV)
0
50
100
150
200
250
10
15
20
25
30
35
40
45
50

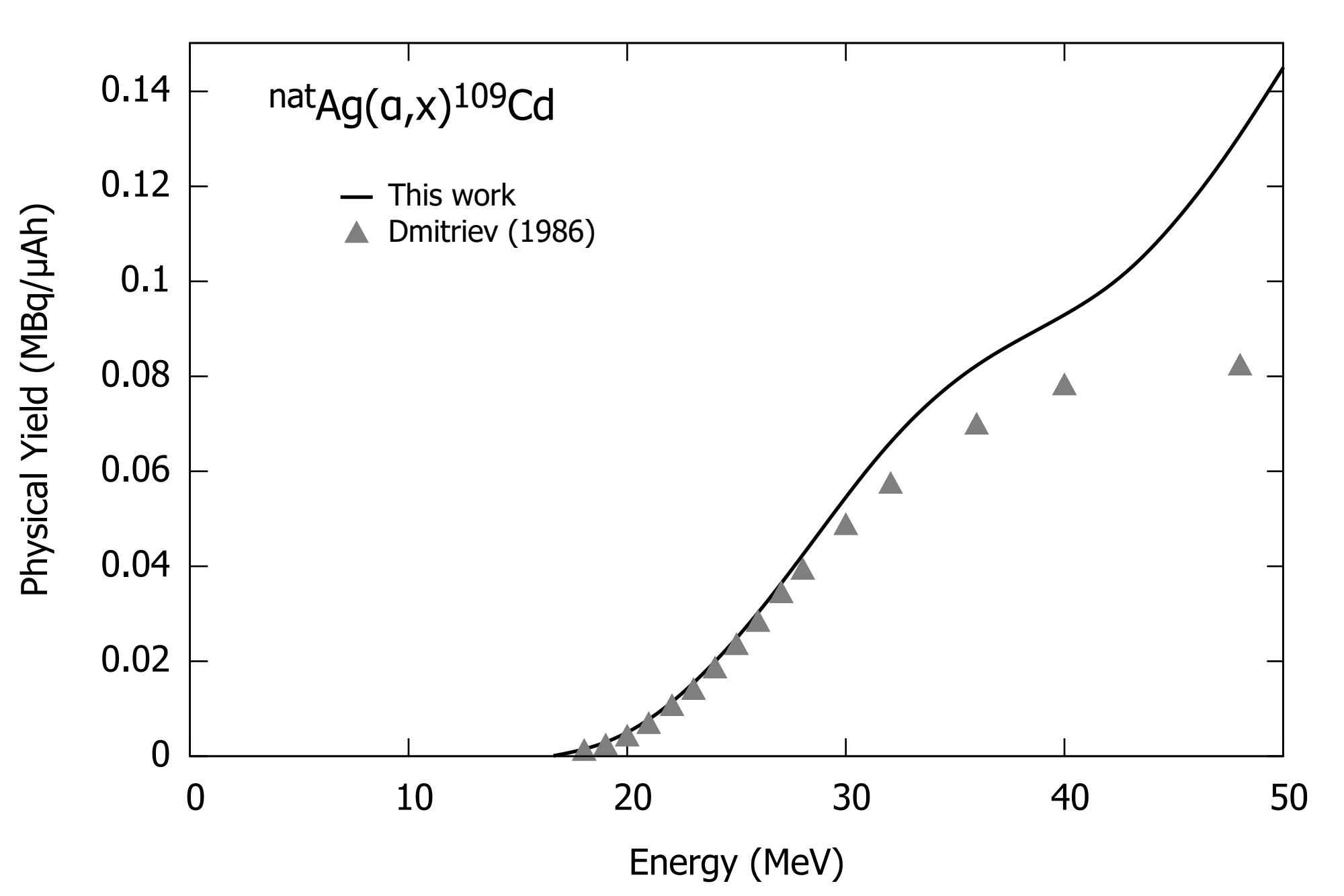
$^{nat}Ag(\alpha,x)^{109}Cd$
This work
Dmitriev (1986)
Physical Yield (MBq/μAh)
Energy (MeV)
0
0.02
0.04
0.06
0.08
0.1
0.12
0.14
0
10
20
30
40
50